Removal of thiophene compounds from model fuel with supported copper on activated carbon, adsorption kinetics, and isotherms

Haleh Golipour
Research Center of Iran
Bahador Kazemi
Research Center of Iran
Morteza Mafi
Research Center of Iran
babak mokhtarani (mokhtaranib@ccerci.ac.ir)
Research Center of Iran

Research Article

Keywords: Activated Carbon, Adsorption, Desulfurization, model fuel, Thiophene compounds

Posted Date: March 2nd, 2023

DOI: https://doi.org/10.21203/rs.3.rs-2603308/v1

Abstract

In this study, the adsorption of thiophene compounds (TCs, comprised of thiophene (T), benzothiophene (BT), and dibenzothiophene (DBT)) from model fuel was performed with modified Active Carbon(AC). The single solute model fuel was prepared at 2000ppm, and the mixture concentration of components was performed for 3000ppm. Furthermore, thiophene adsorption from commercial fuel (kerosene) was studied. Based on the experimental results, the correlated parameters of adsorption isotherms, kinetic models, and Fisher factor were calculated. The pseudo-second-order model has the best fitting to experimental data, and the 10% Cu^{+} supported on acid-washed Activated Carbon (A1CN10) has the best-adsorbed amount of TCs (T, BT, and DBT), being 78, 96, 100%, respectively. The physicochemical characterizations for adsorbents were verified by the N_2 adsorption-desorption surface area analyzer (BET), scanning electron microscopy (SEM), X-ray diffraction (XRD), and Energy Dispersive Spectroscopy (EDS). In addition, the adsorbent-regeneration process was performed by two agitating methods and ultrasound impact was studied.

1. Introduction

Nowadays, thiophene compounds in the fuel have been subjected to severe environmental and health issues. The root cause of acid rain is the SOx compounds, which result from the burning of sulfur compounds in the fuel. The presence of sulfur compounds in fuels leads to the corrosion of pipelines and the poisoning of the catalysts (Mei et al. 2003). Removal of thiophene compounds (thiophene (T), benzothiophene (BT), and dibenzothiophene (DBT) and their derivatives) from gasoline and diesel fuels is an important task.

The European Union has reduced the maximum amount of sulfur in diesel fuel from 2000 to 10 ppmw since 2009. In 2006, the US Environmental Protection Agency(EPA) reduced the sulfur levels in gasoline and diesel to 15 and 30 ppmw, respectively (Al-Lal et al. 2015).

Hydrodesulfurization (HDS) is a common method for the removal of sulfur compounds (including thiols and sulfides) but it is not suitable for the removal of thiophene compounds such as BT, DBT, and their derivatives (Hook and Akgerman 1986). To achieve the limit of sulfur in the fuel and to comply with environmental regulations, the HDS method should be performed at high temperature, and high pressure, while it consumes a lot of hydrogen, so it can give rise to a dramatic increase in the price of the fuel (Lecrenay et al. 1997; Li et al. 2017).

One way to attain global standards and reduce sulfur levels to near zero is to perform the HDS method under severe conditions or apply more economical complementary methods. The insufficiency of the HDS method in removing cyclic compounds has led to utilizing alternative methods. Aromatic compounds may be removed by Extractive Desulfurization (EDS) (Mafi et al. 2018; Mafi et al. 2016; Safa et al. 2016a), Oxidative Desulfurization (ODS) (Dizaji et al. 2019; Khodadadi Dizaji et al. 2018; Safa et al. 2017; Safa et al. 2016b; Seifikar Gomi and Afsharpour 2019), Biological Desulfurization (BDS) (Guobin et al. 2006), desulfurization alkylation-based(Arias et al. 2008), desulfurization chlorine-based (Katritzky et al. 1992), and Adsorption Desulfurization (ADS) (Oloruntoba et al. 2016). However, these methods need to be more investigated.

Among the mentioned methods, ADS might be a suitable method for the removal of sulphur aromatic compounds. The performance of ADS was proved in removing aromatic sulfur compounds under ambient conditions and decreasing the processing time (Ania and Bandosz 2006; Gawande and Kaware 2017; Jin et al. 2020; Khodadadi et al. 2012; Mandizadeh et al. 2018; Nazal et al. 2016). The main advantages of the adsorptive desulfurization process are the availability of the adsorbents used and its low cost, and it does not require expensive conditions as in (HDS) (Ammar 2017). On the one hand, optimization of hydrogen consumption and the production of toxic compounds such as hydrogen sulfide (H_2S) can solve one of the major problems of HDS toward ADS. On the other hand, energy and environmental problems can be solved by optimizing the loss of hydrogen (Magistri et al. 2003).

As the adsorbent is the main and important part of the process and the used adsorbent has a major effect on sulfur removal, many adsorbents are used for this purpose such as activated carbon (AC), zeolites, alumina, amorphous silica, and organic-metal-frameworks(MOFs) have been examined for desulfurization of petroleum samples, naphtha, and gas condensate (Ito and

van Veen 2006). The principal advantage of ADS is the chemical selectivity of adsorbents which depends on the specified sulfur composition in the process. Activated carbon is generally cheaper than most inorganic sorbents and has been reported as a suitable adsorbent for desulfurization (Vilarrasa-García et al. 2010). Shalaby et al. (Shalaby et al. 2009) proposed a continuous process for desulfurization within AC fibers (ACF) that reduces the sulfur content to less than 10 ppm.

By utilization of different treatment processes, such as metal impregnation and oxidation, the adsorbents will be rectified to improve and promote their inclination toward the removal of TC from liquid fuels. In terms of oxidation treatment, modification of AC has been studied through oxidation with HNO_3, H_2O_2, NaOH, $(NH_4)_2S_2O_8$, etc. under relatively mild reaction conditions (eg.,20–100 °C) (Boehm, 2002; Haydar et al., 2003; Hazourli et al., 1994; Moreno-Castilla et al., 1998). Research showed that acid oxidation treatment has a direct influence on the adsorption capacity of ACs (Dehghan and Anbia 2017; Fallah and Azizian 2012; Seredych and Bandosz 2010). To increase the heterogeneity of the adsorbent surface, the presence of surface functional groups, for instance, the acidic oxygen-containing functional groups which can be reached utilizing the oxidant acid treatment, is depicted to be effective and therefore they can enhance the adsorption capacity (Li et al. 2018; Samokhvalov and Tatarchuk 2010). Sano et al. submitted that the oxygen content of carbon materials affects the adsorption capacity and the oxygen content appears to be the reason for their better performance (Sano 2004) Ania et al. also proposed that introducing oxygen-containing groups might facilitate specific oxygen-sulfur interactions; an increase in acidic sites can lead to creating a strain that could become a new active site for adsorption of sulfur compounds (Ania and Bandosz 2005).

On the subject of metal impregnation, more recently, the incorporation of d-block metals (e.g., Ag, Cu, Fe, Ni, and Zn) in different types of adsorbents such as zeolites, silica, and activated carbon has been proposed in a large number of publications (Vilarrasa-García et al. 2010). The combination of metals such as copper and nickel increases selectivity, absorption capacity, and catalytic surface variation. Mousavi et al. (Moosavi et al. 2012) found out that AC, ACF, and hydrogenated ACF can improve the adsorption capacity of model fuels by wet impregnation of metals such as Cu and Ni. Furthermore, they attributed the specific attraction between thiophene compounds, Cu and Ni cations to the π bond.

Moradi et al. (Moradi et al. 2018) adopted a natural zeolite (clinoptilolite) with various modifications. They improved the capability of adsorbing TCs such as DBT and 4-6-DMDBT from model fuel (normal heptane). The ion exchange process using metals such as Cu, Ni, and its hydrogenation increased the capacity of adsorbents. Moreover, the effects of the solvents (n-hexane, n-heptane, and n-decane) on adsorption capacity were investigated. Huo et al. (Huo et al. 2019), utilized bimetallic MOFs to remove DBT from model fuel (n-hexane). They compared the amount of DBT absorption by linking different ratios of the two metals, cobalt, and zinc. Ju et al. (Ju et al. 2019), stabilized nickel oxide and zinc oxide on ion-exchanged zeolite in two nitrogen and hydrogen atmospheres for adsorbing thiophene by reactive absorption on the nickel sites from model fuel (n-hexane). Zhang et al. (Zhang et al. 2019), applied graphene oxide (GO) and reduced graphene oxide (RGO) with varying degrees of reduction to adsorb DBT from model fuel (n-octane). Modifications of various amounts of RGO have enhanced the interaction between the structure of RGO and sulfur composites with π-π bonds. Luo et al. (Luo et al. 2018), prepared activated boron nitride via facile rapid pyrolysis reaction for removal of DBT and had a high performance with 42.2 (mgS/g adsorbent) capacity. The regeneration of the adsorbent was performed in a toluene flask at 60˚C for 30 min and the regeneration method after the fourth replicate had a 65% recovery of adsorbent capacity.

This work aims to investigate the effects of two types of treatment on the adsorption capacity of thiophene compounds in model fuels on AC. The first method, oxidation via two strong acids, and the second method, metal cation impregnation via copper, to study the surface changes and their impact on AC adsorption capacity. Modified activated carbon by loading Cu (I) and Cu (II) was investigated and the selectivity of the adsorbents was studied. Three TCs contains T, BT, and DBT, and the model fuels considered n-hexane, n-heptane, and n-octane. The results of this study showed that the modified AC with Cu cation can be a good choice for the removal of TCs. Their performance in the adsorption of the sulfur-containing compounds from model fuel could be linked up with the pore structure and chemical properties of the AC surface.

2. Material And Methods

2.1. Chemicals and Materials

The chemicals used in this study, their purity, and their suppliers, are summarized in Table 1. AC (purity 99%, cylindrical granules with 1-1.5mm outer diameter and 1-6mm length) was provided by Merck Company. The other base adsorbent used in this study is zeolite molecular sieve 13X granules (Na form) purchased from Zeo-Tech (https://www.zeo-tech.de, CAS no. 1318-02-1) and Zeolite 5A and Y prepared from PP&C (http://www.ppandc.ir). Dibenzothiophene (DBT), Benzothiophene (BT), and Thiophene (T) were applied as sulphur aromatic compounds. Kerosene was purchased from the Ilam Petrochemical Co., Iran, and double-distilled water was used in all experiments.

Table 1
Purity and supplier of materials used in this study

Chemical Name	Supplier	Mass Fraction Purity	Molecular Weight (g/mol)
Dibenzothiophene(DBT)	Merck	> 99%	184.26
Benzothiophene(BT)	Merck	> 99%	134.2
Thiophene(T)	Merck	> 99%	84.14
kerosene	Commercial	-	-
n-Octane	Merck	> 99%	114.232
n-Heptane	Fluka	> 99.5%	100.205
n-Hexane	Romile	> 95%	86.178
Nitric Acid	Merck	> 65%	63.01
Sulfuric Acid	Merck	> 99%	98.079
Copper nitrate trihydrate	Merck	> 99%	241.6

2.2. Adsorbent preparation

AC sample firstly was calcined at 350°C and named AC350. In another procedure, to increase acidic-oxygenated groups on the activated carbon surface, AC was activated by nitric acid (HNO_3) and sulphuric acid (H_2SO_4), which are referred to as ACN and ACS, respectively.

The acid-wash process was performed under similar conditions for both procedures using nitric acid and sulphuric acid. For this modification, the samples were inserted into a 10% acid solution for 3 h and then rinsed with distilled water. After that, the adsorbents were dried in a vacuum oven at 110 ° C for 3 h, and finally, they were calcined at 350°C (Dehghan and Anbia 2017; Deng et al. 2017; Li et al. 2018)

Furthermore, Cu loading on the calcined AC sample using the dry impregnation method was performed by dissolving 2.5 g of Copper nitrate trihydrate ($Cu(NO_3)_2{\cdot}3H_2O$) in 200 ml distilled water, and the solution was refluxed for 3 h at 75°C. For agitating the solutions, the ultrasonic equipment of Elma Schmidbauer GmbH (http://www.elma-ultrasonic.com) P30H model was used. The adsorbent was removed from the solution and washed 3 times and the remaining water was collected to measure the amount of Cu remaining in the solution by using ICP analysis. Then the adsorbent was dried at 120 ° C for 4 hours in a vacuum oven for complete drying and removal of water. Finally, the sample was calcined for 4 h at two different temperatures under the Argon atmosphere due to obtaining different types of Cu cation, Cu(I) and Cu(II). To achieve that, the sample was treated at 270°C to load AC with CuO (Copper(II) oxide) and 480°C to load AC with Cu_2O (Copper(I) oxide) (Moosavi et al. 2012; Morozov et al. 2003). These samples are referred to as A1C (containing Cu(I)) and A2C (containing Cu(II)). Heat treatment temperatures are selected based on the thermal decomposition data of hydrated copper nitrate. In an argon atmosphere, $Cu(NO_3)_2{\cdot}3H_2O$ first melts at 116–152°C, converts to β-$Cu_2(OH)_3NO_3$ at 199–217°C, and decomposes to CuO at 263–310°C. CuO decomposes at > 450°C to Cu_2O and finally decomposes to metallic Cu at higher temperatures (Moosavi et al. 2012).

In the following steps, the 5%, 10%, and 30% Cu^{+} were supported on ACN and named A1CN5, A1CN10, and A1CN30, respectively. Furthermore, the ACN with loading 10% Cu^{+2} was named A2CN10. The 10% wt was chosen because of the optimization measurements explained in the result part of this work.

2.3. Characterization

To investigate the characteristics of prepared sorbents, X-ray diffractometry (XRD) analysis (Philips apparatus, X'pert MPD model) was used for structure detection, qualitative characterization of samples, and to observe changes after loading Cu on AC using Co Kα radiation (λ = 0.154056 nm) at 40 kV in the 2θ ranges of 10°–90°. SEM analysis (Scanning electron microscopy, Tescan-VEGA model) was performed to determine the surface morphology of the adsorbent and perceive active site distribution on the adsorbents. Elemental analysis (EDS analysis, Sirius) was also used to identify the elements' presence and atomic composition in the adsorbent quantitatively and qualitatively. Textural characterization was carried out by measuring the N_2 adsorption isotherms at 77 K using a BELSORP Mini II analyzer. Before the experiments, the samples were outgassed under a vacuum at 200 C for 3 h. The isotherms were used to calculate the specific surface area (a_s), total pore volume (V_T), and pore size distributions. Furthermore, the analysis of the Inductively Coupled Plasma-Optical Emission Spectrometry (ICP-OES, Spectro Model ARCUS) was applied to measuring the loaded Cu on the adsorbent

2.4. Experimental Analysis Procedure

For the adsorption process, 10 ml of the stock solution with a concentration of 2000 ppm of T, BT, DBT, or a mixture of them (3000 ppm) was added to the adsorption column with 2.5 g of adsorbent. The column length and diameter were 11 cm and 2.5 cm, individually. All adsorption experiments were carried out in a fixed-bed column under ambient conditions. The concentration of T, BT, and DBT before and after the desulfurization process was determined with Gas Chromatography (GC, VARIAN CP-3800 model). The GC is equipped with a flame ionization detector and a CP-SIL capillary column with a length of 25 mm, and a diameter of 0.3 mm, and the concentration of TCs was determined with the external standard calibration diagrams. The preliminary tests were conducted to obtain a suitable sampling interval time that fitted the results well to the kinetic models. It should be noted that each test was replicated, at least three times. The model fuels were n-hexane, n-heptane, and n-octane.

To investigate the effects of concentration on the adsorption process and plotting isotherm diagrams for the studied adsorbent, different TCs concentrations were prepared and tested in the calibration concentration range of the adsorption process.

2.5. Adsorption isotherm calculation

Typically, mathematical proportions play an essential role in modeling results, operational design, and figuring out the adsorption system. Over the years, a spectrum of equilibrium isotherm models has been provided and formulated based on differences in the physical interpretation of the parameters utilized in isotherm models (Asgari et al. 2014).

Langmuir's theory is relevant to the accelerated decrease of intermolecular forces and an increase in the distance between the adsorbents. This model is as follows:

$$q_e = \frac{q_m K_L C_e}{K_l C_e + 1}$$

1

In this equation K_L is the Langmuir isotherm equation constant, q_m represents the maximum monolayer coverage, q_e is the equilibrium adsorbed at equilibrium, and C_e is the equilibrium concentration (Ahmad et al. 2017; Khodadadi et al. 2012; Moosavi et al. 2012; Song et al. 2017).

The Freundlich isotherm can be used for multilayer adsorption, with uniform heat dissipation distribution and heterogeneous surfaces. According to the following equation:

$$q_e = K_F C_e^{\frac{1}{n}}$$

2

Where K_F is the Freundlich isotherm constant and n is the adsorption intensity (Ahmad et al. 2017; Danmaliki and Saleh 2017; Song et al. 2017). This equation offers the advantage over Freundlich and Langmuir models due to the consideration of the non-uniformity of solid surface energy (energetic heterogeneity of solid surfaces).

The Redlich-Peterson model which is the most used three-parameter isotherm model is a combination of both Langmuir and Freundlich isotherms that combine the three parameters into an experimental equation. This model is close to the Freundlich model at high concentrations and is ideally close to the Langmuir model at low levels of concentration or ideal state. The equation of this model is as follows:

$$q_e = \frac{K_R C_e}{\alpha_R C_e^g + 1}$$

3

Where g symbolizes the heterogeneity of the adsorbent, is dimensionless, and the values of K_R and α_R are the constants of the Redich-Peterson isotherm (Foo and Hameed 2010). If b is equal to 0, the Redlich-Peterson equation transforms into henry's law and has a linear form. Moreover, when b is equal to 1, the equation is converted to the Langmuir isotherm.

The sips isotherm is a combined form of Langmuir and Freundlich isotherms. In low concentrations, it behaves like the Freundlich model but at high concentrations, it acts like the monolayer Langmuir model. The equation of this model is as follows:

$$q_e = \frac{K_s C_e^{\beta_s}}{a_s C_e^{\beta_s} + 1}$$

4

In this equation, β_s illustrates the power of the Sips isotherm and S_α and K_s are the constants of the Sips isotherm (Agueniou et al. 2018; Foo and Hameed 2010).

3. Results And Discussions

3.1. Characterization of Adsorbents.

The structure and morphology of the surface of the adsorbents are shown in Figs. 1 and 2 with the magnification of 3500x and 350x respectively. The pores of AC in Fig. 1a are comparable to acid-washed AC (b) and the Cu particles on the AC surface are objective (c and d). In Fig. 1 (b and c), the change in pore size of the acid-washed sample before and after Cu(I) stabilization is visible. The main reason for this decline in pore size may be attributed to the dry-inoculation loading using ultrasonic waves. Furthermore, according to Fig. 3, no damage to the pore structure before and after the adsorption process is observed.

To investigate the elements existing on the adsorbent surface, in particular, the presence of Cu, the EDS analysis of the adsorbent with a 10% Cu loading rate was performed and the results are shown in Fig. 3 and Table 2. The presence of C and O elements in all samples depicted in EDS results is related to the structure of AC, and the existence of element Cu on the surface in Fig. 3c confirms the Cu-impregnated samples. In addition, an increase in Oxygen percent can be seen from 8.61% in raw AC to 15.07 in AACN, which is vividly related to the growth of oxygen functional groups. EDS analysis results in the lack and presence of S amount before and after the adsorption operation.

The results of XRD analysis validate the loading of Cu which have a perfect and precise match with EDS analysis.

Table 2
Elemental analysis of samples

Sample	C%	O%	Cu%
Raw AC	91.39	8.61	-
ACN	84.93	15.07	-
A1CN10	83.95	14.96	1.09

The XRD analysis for AC and calcined ACs impregnated with Cu ions (AC-Cu_2O which was referred to as A1C and AC-CuO as A2C) are presented in Figs. 4 and 5.

The crystal structure of the adsorbent and sample identity of the existing elements were determined by XRD analysis. For this purpose, the adsorbents loaded with Cu(I) and Cu(II) have been explained by X-ray irradiation. Mousavi et al (Moosavi et al. 2012) also obtained similar results for this analysis in the loading of Cu(I) and Cu(II) on AC fiber. The X-ray diffraction spectra of AC (base without Cu) are illustrated at the bottom of Figs. 4 and 5. Figure 4 shows the weak and sharp peaks created for the crystalline structure of Cu(II) based on ICDD database standard 0-048-1548 at θ2 angles of 35.54, 38.7, and 56.7 degrees. In Fig. 5, the weak and sharp peaks created for the crystalline structure of Cu(I) are determined by the ICDD database standard No. 2076-078-01, and peaks for Cu(I) were shown at angles of 37, 42.6, and 74.4 degrees. After Cu loading, the peaks associated with AC were observed to be similar, confirming that the basic structure is not degraded. This non-destructive confirmed the validity of the fixation method used.

The structural characteristics of adsorbents and their properties before and after modification are exhibited in Table 3 and N_2 adsorption-desorption isotherms at 77 K are reported in Fig. 6. The BET method was applied for calculating the surface area and the textural properties of the samples containing the BET surface area ($a_{s, BET}$ (m^2 g^{-1})), total pore volume at P/ P0 = 0.99 (cm^3 g^{-1}), average pore diameter (nm), and the observed peak of pore radius ($r_{p, peak}$ (nm)) are listed in Table 3. In Fig. 6, the isotherm shape of all adsorbents according to IUPAC classification demonstrates a typical type I isotherm curve with type H4 hysteresis loops. The adsorption process can be observed even at low relative pressure in type I due to the powerful interactions between adsorbent pores and gas molecules. In addition, the flat line step appeared in a relative pressure range from 0.3 to 0.9 depicting the single-layer adsorption mechanism. Appearing of the Hysteresis loop is usually due to diverse behavior in the adsorption and desorption process. The desorption amount of gas molecules is not as equal to its adsorption amount, so this difference will lead to creating the loop. As can be seen in Fig. 6, the Hysteresis loops are not significant, except for the ACN sample, which can have something to do with its bigger pore size reported in Table 3 due to the acid wash procedure. Also, the Hysteresis loops existing in all curves (H4 type), can be observed in samples consisting of solid constituents and agglomerated in cleft pores (plate shapes or edges such as cubes), uniform in size or shape (Leofanti et al. 1998). As it is depicted in Table 3, the surface area and volume of AC pores were 872.04 m^2g^{-1} and 0.4379 cm^3g^{-1}, and after the acid-wash process, a_s for both ACS and ACN samples has risen to 903.37 and 927.56 m^2g^{-1}. ACN sample also had the biggest average pore diameter and total pore volume among others. On the other hand, after Cu loading (10% wt), these amounts decreased to 733.38 m^2g^{-1} and 0.3534 cm^3g^{-1}, respectively. The most important reason for this may have a relation with coating micro pores surface by impregnating Cu particles. In addition, the pore size distribution has been determined using the adsorption branch of the isotherms and the Barrett – Joyner – Halenda (BJH) method which is depicted in Fig. 7. It is obvious that all samples have a distribution peak in the micropore range being less than 2 nm.

Table 3

Result of BET analysis and structural characterization of samples

Sample	$a_{s,BET}$ (m^2 g^{-1})	Total Pore Volume (p/p_0=0.99)	Average Pore Diameter (nm)	$r_{p,peak}$ (nm)
Raw AC	872.04	0.4379	2.0084	1.21
ACS	903.37	0.4151	2.0188	1.21
ACN	927.56	0.4375	2.1832	1.21
A1Cu	756.69	0.3759	1.9335	1.27
A1CN10	733.38	0.3534	1.9273	1.21
A2Cu	714.51	0.3534	1.9015	1.15

3.2. Adsorption isotherms

The adsorption isotherms and their experimental data for T, BT, and DBT in hexane solvent (T-Hex, BT-Hex, DBT-Hex) on A1CN10 were measured by the procedure explained in section 2.4 and the results are presented in Fig. 8 and Table 4. It can be observed that A1CN10 adsorbed DBT more than other thiophene compounds. The sequence of compound adsorption is DBT > BT > T. This may be according to the more polarity of DBT than BT and T, which can lead to a higher tendency to be adsorbed by Cu ions. All three TC molecules have planar geometries and can orient themselves to enter the AC micropores. However, DBT has a larger molecular cross-sectional area than BT and T, further enhancing its dispersion and π-π interactions with the AC.

The isotherms were correlated with Langmuir, Freundlich, Sips, and Redlich-Peterson isotherms using the Matlab software.

Table 4

Experimental data for T, BT, and DBT on A1CN10 in Hexane solvent

Model Fuel	T- Hex		BT- Hex		DBT- Hex	
	C_e (mgS/L)	q_e (mgS/gAdsorbent)	C_e (mgS/L)	q_e (mgS/gAdsorbent)	C_e (mgS/L)	q_e (mgS/gAdsorbent)
	0	0	0	0	0	0
	222.356	0.848	19.595	4.625	1.170	4.639
	784.072	6.802	127.59	9.313	2.970	10.235
	1802.901	9.915	1857.5	13.193	290.97	15.475
	2934.682	12.313	2112.5	19.093	2230.9	20.115
	3922.689	13.979	5545.5	19.641	5630.9	22.115
	5409.124	15.532				

The calculation of adsorption isotherm was performed by the Curve Expert (Version 2.6.3) program. The software uses nonlinear least-square fitting of the averaged experimental data by using the Marquardt-Levemberg algorithm. The algorithm seeks the values of the parameters that minimize the sum of the square differences (SSD) between the experimentally measured values (q_{exp}) and calculated values of the dependent variable by the model being studied (q_t) (Panahi 2008):

$$SSD = \sum_{i=1}^{n} \left(q_{\exp i} - q_{ti}\right)^2$$

5

Where n is the number of experimental data points. For fitting the single-component adsorption isotherm data, the identification process was carried out several times.

The selection of sufficient adsorption isotherm models and their accuracy in fitting performance was carried out using the Fisher parameter (f). According to this factor, the model with better correlation data is the one that exhibits the highest value of the Fisher parameter, defined as:

$$f = \frac{(n-p)\sum_{i=1}^{n}\left(q_{\exp i} - \bar{q}_{exp}\right)^2}{(n-1)\sum_{i=1}^{n}\left(q_{\exp i} - q_{ti}\right)^2}$$

6

Where n is the number of experimental data points, p is the number of adjusted parameters of the model, and $\bar{q}_{exp}$ is the average of the experimental data points (Baggiani et al. 2004).

According to the Fisher test results, each model is suitable for one solute, Langmuir for T with a higher f factor than others (138.61 on AC and 48.523 on A1CN10), Sips for BT on AC (139.64) and Freundlich for BT on A1CN10 (34.46), Redlich-Peterson for DBT (117.70 on AC and 16.45 on A1CN10) showed the best fitting to experimental data (Tables 5 and 6).

Table 5
Freundlich and Langmuir parameters, correlation coefficient, and Fisher factor for T, BT, and DBT adsorption on AC and A1CN10 in Hexane solvent

	Sample	**AC**			**A1CN10**		
	Material	**T**	**BT**	**DBT**	**T**	**BT**	**DBT**
Isotherm Model	Model Parameter						
Langmuir	K_L	0.000532	0.0130	0.17004	0.0005	0.00926	0.32
	q_m	9.425	12.17	18.35	21.18	17.87	19.39
	R_2	0.994	0.774	0.907	0.983	0.858	0.889
	SSD	0.189	13.567	16.515	2.401	23.4	22.756
	f	138.61	3.3303	8.0758	48.523	5.2932	6.7898
Freundlich	K_F	0.121	2.703	6.5307	0.179	2.97	6.98
	n	2.1178	5.7352	7.363	1.9045	4.851	7.37
	R^2	0.969	0.991	0.951	0.951	0.987	0.945
	SSD	1.002	0.504	8.547	7.044	3.594	11.308
	f	26.27	89.55	15.6	16.54	34.46	13.66

Table 6
Redlich-Peterson and Sips parameters, correlation coefficient, and Fisher factor for T, BT, and DBT adsorption on AC and A1CN10 in Hexane solvent

	Sample	**AC**			**A1CN10**		
	Material	T	BT	DBT	T	BT	DBT
Isotherm Model	Model Parameter						
Redlich-Peterson	g	1.004	0.825	0.909	1.034	0.818	0.907
	K_R	0.00499	6138348	8.747	0.0101	1.137	12.66
	α_R	0.00051	2270187	0.9398	0.00035	0.3073	1.29
	R_2	0.9942	0.9916	0.9957	0.9836	0.9822	0.9696
	SSD	0.1899	0.5045	0.7554	2.3899	2.9376	6.2603
	f	103.98	59.703	117.7	36.57	28.11	16.45
Sips	β_s	1.0415	0.06414	0.34677	1.6653	0.2272	0.2286
	K_s	0.00381	2.0347	6.764	0.00014	2.8572	7.913
	α_s	0.00042	0.40572	0.2867	8.9E-06	0.02122	0.2214
	R^2	0.994	0.9964	0.9838	0.9745	0.9784	0.9519
	SSD	0.19533	0.2157	8.5471	3.7109	3.5641	9.9119
	f	101.1	139.64	30.93	23.55	23.17	10.39

3.3. Adsorption kinetics

One of the important inquiries in the adsorption process is to investigate kinetic studies to determine the equilibrium time. Adsorption kinetics illustrates the pathway of the adsorption process to equilibrium by defining the physical and chemical features of the adsorbent surface concerning the adsorbed molecules and also determines the residence time required for a complete adsorption reaction. Therefore, the study of adsorption kinetics can be contemplated as one of the most influential agents for designing a fitting adsorption system. Kinetic data can be used to determine the dimensions of systems, fixed bed components, or any other streaming system. In this work, the mechanism of the adsorption system including physical and chemical adsorption was studied by pseudo-first-order, pseudo-second-order, and Elovich models (Khajeh Amiri et al. 2019; Nazal et al. 2016). The equations of these models are summarized in Table 7.

Table 7
Summaries of kinetic model equations

Model	**Equation**
Pseudo-first-order	$\log(q_e - q_t) = \log(q_e) + \frac{K_1}{2.303} t$
Pseudo-second-order	$\frac{t}{q_t} = \frac{1}{K_2 q_e^2} + \frac{1}{q_e} t$
Elovich	$q_t = \frac{1}{b} \ln(ab) + \frac{1}{b} \ln(t)$

In the above equations presented in Table 7, the K_1 (s^{-1}) and K_2 (mg/g.s) are the quadratic reaction rate constants, and a and b are the constants of the Elovich model. The amount of Adsorbed substance at the equilibrium moment is q_e (mgS/ g), and q_t (mgS/ g) is the amount of absorbed substance at time t (Alkan et al. 2007; Li et al. 2018). The results of adsorption kinetic models are reported in Tables 8 and 9, and the pseudo-second-order model seems to be the best model fitting ACN and A1CN10 in the n-hexane as the solvent for each of the TCs. The pseudo-first-order, pseudo-second-order, and Elovich kinetic models for the hexane-thiophene solution on ACN as a sample of kinetic modeling results are shown in Fig. 9.

Table 8
Results of pseudo-first-order and pseudo-second-order kinetic models for T, BT, and DBT in heptane and hexane solvents using AC, ACN, and A1CN10

	Model	**Pseudo-first-order**			**Pseudo-second-order**		
Adsorbent	Solution	K_1	q_e	R^2	K_2	q_e	R^2
AC	Hex-T	0.1524	1.9652	0.8485	154.23	6.1254	0.9966
	Hex-BT	0.0325	2.3341	0.8873	203.154	7.8751	0.9999
	Hex-DBT	0.0452	1.0253	0.7583	2256.454	8.7212	1
ACN	Hex-T	0.2733	2.5245	0.8551	128.355	6.6245	0.9998
	Hex-BT	0.0264	2.5462	0.8742	185.236	8.8001	0.9999
	Hex-DBT	0.0385	1.2215	0.7535	3015.246	8.8564	1
A1CN10	Hex-T	0.2374	2.7283	0.8246	113.496	7.0175	0.9999
	Hex-BT	0.0223	2.9046	0.8466	179.535	8.8261	0.9999
	Hex-DBT	0.0403	1.4511	0.5185	2988.933	9.0663	1
	Hep-T	0.0267	3.4047	0.9327	51.106	6.3371	0.9997
	Hep-BT	0.0289	3.453	0.8146	277.059	8.9605	0.9999
	Hep-DBT	0.0497	1.4986	0.8346	1118.848	8.5251	1

Table 9
Results of the Elovich kinetic model for T, BT, and DBT in heptane and hexane solvents using AC, ACN, and A1CN10

		Elovich Model		
Adsorbent	Solution	a	b	R^2
AC	Hex-T	12.454	1.1084	0.9584
	Hex-BT	98.659	1.1547	0.8579
	Hex-DBT	102458.215	2.0023	0.7856
ACN	Hex-T	15.689	1.1526	0.9442
	Hex-BT	178.614	1.2254	0.8692
	Hex-DBT	198745.685	2.2156	0.7721
A1CN10	Hex-T	22.355	1.1631	0.9284
	Hex-BT	281.822	1.2178	0.8579
	Hex-DBT	249514.554	2.3941	0.7255
	Hep-T	7.928	1.1621	0.9754
	Hep-BT	251.596	1.2001	0.9561
	Hep-DBT	683935.118	2.1417	0.8031

The experiments were performed under completely identical conditions (considering the amount of adsorbent consumed and solution employed in the column, the concentration of each solution of thiophene compounds).

After loading Cu(I) on the calcined AC adsorbent, the adsorption kinetics at different concentrations of thiophene was examined. The calculated parameters of the kinetic models for the removal of thiophene in a solution containing a mixture of n-hexane and n-heptane on A1CN10 are shown in Tables 10 and 11. Each model had different feedback on fitting data at different concentrations. The best-fitting result was related to the pseudo-second-order kinetic model, which showed that the different concentration ranges of solvent in each chosen model fuel did not have a significant effect on this kinetic model, and it is useful in any concentration.

Table 10
Results of pseudo-first-order and pseudo-second-order kinetic models for thiophene in the mixture of heptane and hexane solvents using A1CN10

Kinetic Model	Pseudo-first-order			Pseudo-second-order		
Concentration	K_1	q_e	R^2	K_2	q_e	R^2
1000ppm	0.11676	1.77541	0.9875	11.21968	2.98507	0.9997
2000ppm	0.11146	6.4804	0.9765	258.162	8.0581	0.9984
5000ppm	0.17272	10.8243	0.9844	801.887	12.8369	0.9975
7000ppm	0.18101	16.5272	0.9133	1860.494	17.6056	0.9988
10000ppm	0.15936	15.7108	0.9204	2593.769	18.5873	0.9997

Table 11
Results of Elovich kinetic model for thiophene in the mixture of heptane and hexane solvents using A1CN10

	Elovich Model		
Concentration	a	b	R^2
1000ppm	4.7492	2.0981	0.9357
2000ppm	13.4367	0.7437	0.9232
5000ppm	17.1347	0.4631	0.9331
7000ppm	5.4445	0.2447	0.9223
10000ppm	22.1899	0.3134	0.9475

3.4. Effect of model fuel in thiophene compounds adsorption

The impact of fuel type on the removal of thiophene compounds (T, BT, and DBT) in n-hexane, n-heptane, and n-octane as model fuels were investigated under the same conditions (2000 ppm initial concentration for T, BT, and DBT, in 4 different times, 60, 120, 180, and 240 minutes using AC sample) to confirm the interactions between model fuels and the removal of thiophene compounds. The consequences of these experiments illustrated that the removal of T, BT, and DBT increased by growth in molecular fuel weight (Kumagai et al. 2010; Moradi et al. 2018). As a result, DBT had the highest removal percentage among others and the rate of removal of T had a direct correlation to its lower molecular weight in comparison to BT and DBT. Each of these data that are presented in Table 12 is the average of three replications. Similar relation can be seen between the molecular weight of the solution and the removal percentage. Each model fuel had the biggest removal amount in the n-octane solution which had the most weight and n-heptane and n-hexane was the next selection respectively.

Table 12
Removal percentage of T, BT, and DBT by AC in Hexane, Heptane, and Octane model fuel

		Removal Percentage in Exact Time(%)			
Component	Model fuel	60min	120min	180min	240min
T	n-Octane	50.2	50.4	50.6	50.58
	n-Heptane	44.23	44.26	44.26	44.26
	n-Hexane	39.81	39.9	39.96	39.96
BT	n-Octane	72.78	72.8	72.8	72.8
	n-Heptane	69.33	69.4	69.4	69.4
	n-Hexane	66.26	66.29	66.29	66.29
DBT	n-Octane	91.25	91.25	91.25	91.25
	n-Heptane	88.2	88.2	88.2	88.2
	n-Hexane	86.1	86.1	86.1	86.1

3.5. Effect of different treatments on adsorption capacity and thiophene compounds removal

The first experiment included a comparison between four samples, 3 types of Zeolites (Y,13X,5A), and AC. This series of tests were examined in a batch reactor for 120 min under ambient conditions to choose the best base adsorbent. Normal heptane as the model fuel was selected based on having the more difficult removal of thiophene compared to normal hexane and the results are presented in Table 13. Based on these measurements, it seems to be that AC is a better adsorbent rather than zeolite samples due to possessing a higher thiophene removal concentration (932 ppm). After AC, the sequence of thiophene removal among zeolites is Y > 5A > 13X.

Table 13
Removal percentage of 2000ppm thiophene from n-heptane using 4 different types of adsorbents

Adsorbent	Removal Concentration (ppm)	Removal Percentage (%)
AC	932	46.6
Zeolite 13X	538	26.9
Zeolite 5A	602	30.1
Zeolite Y	684	34.2

Following the treatments labeled in section 2.2, some adsorption experiments were applied to AC to remove thiophene from n-hexane. The adsorption capacity and rate in each treatment were examined and the results are presented in Figs. 10 to 12. Each treatment had distinct effects on adsorption capability and activated surface. This enhancement in the removal of thiophene can be described by the abandonment of some composites and interstitial water in the sorbent. After drying, the next step was the addition of Copper nitrate solution to the adsorbent, and the Cu metal was stabilized as Cu(I) and Cu(II) ions on the adsorbent by calcination in different temperatures (dry impregnation method). The results of this treatment on thiophene removal in n-Hexane on adsorbents A1C and A2C during 60 minutes are reported in Fig. 10 and their curves were compared to AC and calcined AC (AC350). The results of Fig. 10 indicated that the presence of Cu ions improved sulfur compounds' affinity through AC according to both physical and chemisorption uptakes. Moreover, the existence of Cu(I) displayed more activity than Cu(II) since A1C had a higher removal percentage than A2C (approximately 61.9% and 58.9% respectively). Cu(I) cation has a higher elasticity toward sulfur uptake(Moosavi et al. 2012). As the adsorption kinetics shows, Cu(I) also improved the removal rate too. Adsorbents can remove more TCs maybe by having a pi-bond between Cu ions and thiophene. In addition, according to the hard and soft acid and bases (HSAB) theory, the presence of sulfur atoms that can act as soft bases will cause a favorable interaction with copper cations which can act as soft acids (Eslami et al. 2011).

Furthermore, the behavior of acid-washed samples (ACN and ACS) was compared with AC and AC350 samples, and their thiophene removal percentage curves during 60 minutes are shown in Fig. 11. The results indicated that the acid-washing procedure was much more effective than dry-inoculation and also calcification, as both ACS and ACN samples showed a higher removal percentage (nearly 73.5 and 68.5 percent) than AC, AC350, A1C, and A2C.

First, introducing oxygen-containing groups might facilitate specific oxygen-sulfur interactions. A rise in acidic sites also disturbs the charge distribution of the carbon surface and creates strain that plays as a new active site for the adsorption process, which would interact more favorably with the basic sulfur compounds. Second, the presence of acidic sites in the carbon structure might create favorable interactions with the sulfur compounds. The presence of acid groups on the carbon surface as a result of the acid-washing process is beneficial to thiophene compounds and it may have a direct correlation to the growth in the heterogeneity of the adsorbent surface and therefore they can enhance the adsorption capacity. The more interaction between the acidic centers of the modified samples and the basic groups of organosulfur compounds, the higher the adsorption capacity will be. In addition, the best results of three sorts of treatments can be seen in Fig. 12, which is a comparison between them and

raw AC to see the performance of samples, including A1C (the sample with the better result using dry impregnation method), ACN (the sample with the better result using the acid-washing method) and A1CN10 (the sample modified by both methods).

To evaluate the results obtained from the commercial fuel model, the removal of thiophene from the real fuel was examined. For this purpose, the kerosene was chosen and the total amount of sulfur was measured by X-ray fluorescence spectrometer with the RIGAKU NEX QC + model twice, before and after the adsorption procedure. This analysis was performed according to the ASTM4294 standard and each analysis was repeated twice. The total sulfur amount was 1420 initially. Then thiophene with a concentration of 2000 ppm was added to this fuel. The removal percentage of thiophene in 60 minutes was performed and the final amount of the thiophene analyzed by GC was equal to 840 ppm and the final total sulfur value was 970 ppm. The removal percentage changes are depicted in Fig. 13. Despite the full range of compounds present in kerosene, the adsorbent performed well and eliminated 58% of 2000 ppm thiophene that was added to kerosene and after the adsorption process, the total sulfur amount reduced from 3420 ppm to 970 ppm.

3.5.1. Effect of Cu Loading

A1CN5, A1CN10, and A1CN30 are three adsorbents that were loaded 5, 10, and 30 wt% of Cu(I) on ACN, respectively. To calculate the amount of Cu(I) loaded on those samples, the amount of Cu(I) that remained in the solution after the dry impregnation operation which was measured by ICP analysis, was subtracted from the original solution concentration. On the other hand, by altering the weight of the adsorbent before and after impregnation, the amount of preserved Cu(I) will be obtained. The experimental section was performed on a hexane-thiophene solution for all three adsorbents. The results are displayed in Fig. 14.

It can be seen in Fig. 14 that A1CN10 adsorbent shows the highest removal percentage among other samples by removing approximately 80% of thiophene after 120 minutes.

Moreover, this treatment (Cu impregnation) improved the adsorbent performance and the result indicated that the appropriate Cu loading percentage is 10% with the adsorption capacity equal to 7.79 mgS/g and it seems that the A1CN10 sample has the optimum Cu loading percentage since 30%-Cu loading declined the adsorbent capacity to 5.6 mgS/g.

3.6. Adsorbent selectivity

To evaluate the adsorbent performance and selectivity in a solution containing all three kinds of TCs, a series of experiments were carried out as follows in Table 14 and the removal percentage of mixture components (T, BT, and DBT) in n-hexane on A1CN10 is depicted in Fig. 15.

Table 14
Results of the removal of mixture TCs by different adsorbents in n-Hexane

Adsorbent	Removal Percentage (%)		
	T	BT	DBT
AC	36	71	97
A2C	48	79	99
ACS	50	85	99
ACN	58	94	100
A1CN10	69	98	100

As shown in Table 14, the adsorption capacity of TCs on A1CN10 and ACN adsorbents was higher than in other samples. All samples removed DBT more than BT and T in the mixture and the A1CN10 adsorbent vividly indicated the best action in removing T, BT, and DBT. The lowest and highest DBT removal percentage among these adsorbents were 97% for AC and 100%

for two samples (ACN and A1CN10), respectively. Whereas the removal amount for BT was 98% in the best performance (A1CN10) and 71% in the weakest one (AC), individually. The same is true of thiophene.

The distribution coefficient K_d (litre/g) is calculated for each component based on the following equation (Nazal et al. 2016):

$$\mathrm{K}_d = \frac{Q_e}{C_e}$$

7

In this equation Q_e is the equilibrium adsorption capacity (mgS/g) and C_e is the concentration of thiophene compounds in the sample fuel (mg/l) at the equilibrium point. The distribution coefficient is used in the calculation of the selectivity factor (K) for the DBT over the (i) component which follows the equation below and the results are listed in Table 15:

(8) $K_s = \frac{\mathrm{K}_d(\mathrm{DBT})}{\mathrm{K}_d(\mathrm{i})}$

In this equation, K_s is the selectivity factor, and the suffix i is referred to the molecules being compared (T or BT) (Nazal et al. 2016).

Table 15
Adsorbents Selectivity

	Adsorbent					
	AC			A1CN10		
	Q_e	K_d	K_s	Q_e	K_d	K_s
DBT	3.85	0.0039	1	3.97	0.004	1
BT	3.33	0.0028	1.393	4.58	0.0039	1.026
T	1.85	0.0014	2.786	3.54	0.0027	1.481

The selectivity of the TCs was: T < BT < DBT, by using Eq. 8 and adsorbents have less tendency to adsorb T than BT and BT than DBT. Furthermore, the AC sample was more selective than A1CN10 despite having the lowest removal percentage among all adsorbents. The selectivity factor for DBT over BT and DBT over T can be expressed in three aspects of feasibility. Firstly, the pore size is close to the size of the DBT molecules. As a result, it leads to allow the DBT molecules to fall into the better trap of the adsorbent pores. The second factor is related to having a higher dipole moment amount, molar mass, and aromaticity level for DBT which can create a stronger Van der Waals bond and π-π interaction with the adsorbent surface. The third factor is the lower basicity of T and BT toward DBT which causes a weaker acid-base interaction with copper oxide (Lewis acid) on the adsorbent surface.

The adsorption capability of the initial adsorbent for n-hexane was 3.54, 4.63, and 4.8 (mgS/g adsorbent) for T, BT, and DBT, respectively. In the study of sample fuel by combining T, BT, and DBT in the n-heptane solvent, the results indicated that the selectivity of the adsorbent was similar to the above process.

3.7. Regeneration

In the investigation of regeneration feasibility in existing methods, a combination of two approaches, using solvent and thermal operation, was used to regenerate the samples. The first step of the procedure was adding the adsorbents to the solvent (n-heptane) and immersing them in it along with stirring at 70°C. In addition, to examine the effect of different types of stirring in the recovery phase, two approaches were chosen containing using rotary (for 6 hours at 150 rpm) and also ultrasonic waves (100 KW power, 37 KHz frequencies, and pulse wave type) to regenerate and stir adsorbent in the solvent. The reason for choosing these conditions is to have a safe and simple way to catch fine adsorbent structures and prevent them from being crushed.

Furthermore, the experiments indicated that the regeneration percentage has a direct relation with the increase in temperature, and the highest temperature before the solvent's boiling point should be chosen. As a result, 70 °C was chosen considering the heptane boiling point. Then, the adsorbent was dried under the ambient temperature for a day and finally, the adsorbents were heated in the vacuum oven at 110°C for 4 hours to be refreshed. Adsorbents were reserved in a desiccator for utilization in the next experiments. Farag et al (Farag 2007) performed similar operations with toluene solvents, n-octane for adsorbent regeneration, and also Wang et al (Wang and Yang 2007), investigated the impact of ultrasonic waves on recovery in a solvent consisting of n-octane and benzene. The results of the removal percentage of thiophene by AC, the adsorbent capacity, and recovery percentage in 5 steps (fresh AC, and first to fourth recovery) during 40 minutes are listed in Table 16.

Table 16

Capacity, removal, and recovery percentage of thiophene by AC using different methods for four-time regeneration

		Removal Percentage in Exact Time(%)									
Regeneration	Agitate Method	1min	5min	7min	10min	15min	20min	30min	40min	Capacity (mgS/g)	Recovery (%)
Fresh	Rotary	27.63	49.37	53.73	59.15	62.20	66.22	73.09	73.29	7.176	-
	Ultra-sound	28.71	50.28	55.90	60.73	67.99	71.15	73.05	73.11	7.296	-
1st	Rotary	12.98	36.07	40.62	45.25	49.75	52.53	52.96	52.96	4.535	63.20
	Ultra-sound	20.54	42.02	47.94	52.87	58.29	60.57	62.04	62.04	6.222	85.28
2nd	Rotary	9.49	24.07	32.96	39.73	46.91	49.98	52.33	52.33	4.324	60.25
	Ultra-sound	18.84	37.71	42.53	47.02	52.16	54.76	56.87	59.89	5.264	72.14
3th	Rotary	9.26	23.56	31.22	37.05	45.24	48.59	50.32	50.32	4.129	57.54
	Ultra-sound	18.86	24.61	41.86	45.44	51.16	55.32	57.19	57.19	5.214	71.47
4th	Rotary	5.46	22.02	29.71	34.80	44.12	47.23	48.64	48.64	4.104	57.19
	Ultra-sound	18.80	25.21	42.16	46.26	50.78	54.83	55.63	55.63	5.207	71.37

As mentioned in Table 16, ultrasonic waves and rotary regenerated 85.28% and 63.20% of the sample adsorption capacity in the first phase of recovery, respectively. The ultrasonic waves as the more efficient method reduced the initial solution from 2000 ppm to 690 ppm. The adsorbent removal capacity in this work was 7.29 $mgS/g_{adsorbent}$ in the initial experiment and it has a capacity equal to 6.22 $mgS/g_{adsorbent}$ after the initial recovery operation, which accounts for about 85% of the first capacity. The adsorbent regeneration was repeated four times as mentioned before. The removal capacity of the adsorbent reached an almost constant value after the second recovery and after the fourth recovery, regeneration was 71.5% of the initial solution from a concentration level of 2000 ppm to 809 ppm. In addition, the recovery percentage after the fourth step using the rotary was about 57%. As a result, these data showed that ultrasonic waves had more impact on fraction bonds between sulfur and adsorbent surface by having 22% recovery more than rotary in just one set.

4. Conclusion

Among four types of investigated adsorbents (AC, zeolite type 5A, 13X, and Y), AC has the best result in removing thiophene from the solution. Furthermore, A1CN10 had the best performance among other modifications comprising acid-washed and copper-impregnated samples. The thiophene (T), benzothiophene (BT), and dibenzothiophene (DBT) adsorption capacities on A1CN10 were 7.79, 9.4, and 10.2 mgS/g, respectively. Among all kinetic models fitted by the experimental data, the pseudo-second-order

equation depicted a better fitting than the other equations within the equilibrium time, regardless of the type of AC and solvent. The importance of isotherm models obtained by the Fisher factor was proved that the Langmuir isotherm for thiophene, the Freundlich isotherm for benzothiophene, and the Redlich-Peterson for dibenzothiophene on A1CN10 had the better performance. It has been seen that this parameter was different for each component. The different types of solvents with different weights had an influence on TCs adsorption capacity and a greater TCs adsorption amount was observed for AC in n-hexane than in n-heptane and n-octane. The removal percentages of the mixture of T, BT, and DBT were 69%, 98%, and 100% for A1CN10, respectively. In solvent-thermal-assisted regenerating, the effect of ultrasonic waves on recovered adsorbent capacity was investigated. AC sample reached 63% and 85% of the initial adsorbent capacity during mixing with the rotary evaporator and by using ultrasonic waves under the same conditions. As a consequence, using ultrasonic waves increased 22% of the recovered capacity in comparison to using rotary.

Declarations

Ethical Approval

The authors have no relevant financial or non-financial interests to disclose.

Competing interests

I declare that the authors have no competing interests as defined by Springer, or other interests that might be perceived to influence the results and/or discussion reported in this paper.

Authors' contributions

Haleh Golipour, prepared experimental setup & wrote the main manuscript

Bahador Kazemi, performed experimental measurement

Morteza Mafi, prepared figures and edited the main manuscript, modelling.

Babak Mokhtarani, supervised and management the project, final editing

Funding

There is no funding for this research.

Availability of data and materials

All data for this research are available upon of request.

References

1. Agueniou, F., Chebli, D., Bouguettoucha, A., Reffas, A., sekirifa, M.L., Baameur, L., Amrane, A.: Removal of tiemonium methylsulfate, from aqueous solutions using activated carbon prepared from date stones. Part. Sci. Technol. 6351, 1–10 (2018).
2. Ahmad, W., Ahmad, I., Ishaq, M., Ihsan, K.: Adsorptive desulfurization of kerosene and diesel oil by Zn impregnated montmorollonite clay. Arab. J. Chem. 10, S3263–S3269 (2017).
3. Al-Lal, A.-M., Bolonio, D., Llamas, A., Lapuerta, M., Canoira, L.: Desulfurization of pyrolysis fuels obtained from waste: Lube oils, tires and plastics. Fuel. 150, 208–216 (2015).
4. Alkan, M., Demirbaş, Ö., Doğan, M.: Adsorption kinetics and thermodynamics of an anionic dye onto sepiolite. Microporous Mesoporous Mater. 101, 388–396 (2007).
5. Ammar, S.: Adsorption Kinetic and Isotherms Studies of Thiophene Removal from Model Fuel on Activated Carbon Supported Copper Oxide. Iraqi J. Chem. Pet. Eng. 18, 83–93 (2017).

6. Ania, C.O., Bandosz, T.J.: Importance of Structural and Chemical Heterogeneity of Activated Carbon Surfaces for Adsorption of Dibenzothiophene. Langmuir. 21, 7752–7759 (2005).
7. Ania, C.O., Bandosz, T.J.: Metal-loaded polystyrene-based activated carbons as dibenzothiophene removal media via reactive adsorption. Carbon N. Y. 44, 2404–2412 (2006).
8. Arias, M., Laurenti, D., Geantet, C., Vrinat, M., Hideyuki, I., Yoshimura, Y.: Gasoline desulfurization by catalytic alkylation over silica-supported heteropolyacids: From model reaction to real feed conversion. Catal. Today. 130, 190–194 (2008).
9. Asgari, M., Anisi, H., Mohammadi, H., Sadighi, S.: Designing a commercial scale pressure swing adsorber for hydrogen purification. Pet. Coal. 56, 552–561 (2014).
10. Baggiani, C., Giraudi, G., Giovannoli, C., Tozzi, C., Anfossi, L.: Adsorption isotherms of a molecular imprinted polymer prepared in the presence of a polymerisable template Indirect evidence of the formation of template clusters in the binding site. 504, 43–52 (2004).
11. Boehm, H.P.: Surface oxides on carbon and their analysis: A critical assessment. Carbon N. Y. 40, 145–149 (2002).
12. Danmaliki, G.I., Saleh, T.A.: Effects of bimetallic Ce/Fe nanoparticles on the desulfurization of thiophenes using activated carbon. Chem. Eng. J. 307, 914–927 (2017).
13. Dehghan, R., Anbia, M.: Zeolites for adsorptive desulfurization from fuels: A review. Fuel Process. Technol. 167, 99–116 (2017).
14. Deng, L., Lu, B., Li, J., Lv, G., Du, S., Shi, J., Yang, Y.: Effect of pore structure and oxygen-containing groups on adsorption of dibenzothiophene over activated carbon. Fuel. 200, 54–61 (2017).
15. Dizaji, A.K., Mokhtarani, B., Mortaheb, H.R.: Deep and fast oxidative desulfurization of fuels using graphene oxide-based phosphotungstic acid catalysts. Fuel. 236, 717–729 (2019).
16. Eslami, S., Mousavi, S.M., Danesh, S., Banazadeh, H.: Modeling and simulation of CO_2 removal from power plant flue gas by PG solution in a hollow fiber membrane contactor. Adv. Eng. Softw. 42, 612–620 (2011).
17. Fallah, R.N., Azizian, S.: Removal of thiophenic compounds from liquid fuel by different modified activated carbon cloths. Fuel Process. Technol. 93, 45–52 (2012).
18. Farag, H.: Selective adsorption of refractory sulfur species on active carbons and carbon based CoMo catalyst. J. Colloid Interface Sci. 307, 1–8 (2007).
19. Foo, K.Y., Hameed, B.H.: Insights into the modeling of adsorption isotherm systems. Chem. Eng. J. 156, 2–10 (2010).
20. Gawande, P.R., Kaware, J.P.: Review on -Regeneration of Activated Carbon. 3, 499–501 (2017).
21. Guobin, S., Huaiying, Z., Jianmin, X., Guo, C., Wangliang, L., Huizhou, L.: Biodesulfurization of hydrodesulfurized diesel oil with Pseudomonas delafieldii R-8 from high density culture. Biochem. Eng. J. 27, 305–309 (2006).
22. Haydar, S., Ferro-García, M.A., Rivera-Utrilla, J., Joly, J.P.: Adsorption of p-nitrophenol on an activated carbon with different oxidations. Carbon N. Y. 41, 387–395 (2003).
23. Hazourli, S., Bonnecaze, G., Astruc, M.: Influence de divers traitements sur les groupements oxygenes superficiels et le potentiel d'un charbon actif en grains. Carbon N. Y. 32, 523–535 (1994).
24. Hook, B.D., Akgerman, A.: Desulfurization of dibenzothiophene by in-situ hydrogen generation through a water gas shift reaction. Ind. Eng. Chem. Process Des. Dev. 25, 278–284 (1986).
25. Huo, Q., Li, J., Liu, G., Qi, X., Zhang, X., Ning, Y., Zhang, B., Fu, Y., Liu, S.: Adsorption desulfurization performances of Zn/Co porous carbons derived from bimetal-organic frameworks. Chem. Eng. J. 362, 287–297 (2019).
26. Ito, E., van Veen, J.A.R.: On novel processes for removing sulphur from refinery streams. Catal. Today. 116, 446–460 (2006).
27. Jin, M., Hu, B., Tang, X., Zou, L., Yu, G.: Effect of Activation Condition on the Performance of Activated Sludge Carbon-Based Adsorbent in Diesel Desulfurization. IOP Conf. Ser. Earth Environ. Sci. 446, 032054 (2020).
28. Ju, F., Wang, M., Wu, T., Ling, H.: The Role of NiO in Reactive Adsorption Desulfurization Over NiO/ZnO-Al_2O_3-SiO_2 Adsorbent. Catalysts. 9, 79 (2019).
29. Katritzky, A.R., Balasubramanian, M., Siskin, M.: Aqueous high-temperature chemistry of carbo- and heterocycles. 17. Thiophene, tetrahydrothiophene, 2-methylthiophene, 2,5-dimethylthiophene, benzo[b]thiophene, and dibenzothiophene.

Energy & Fuels. 6, 431–438 (1992).
30. Khajeh Amiri, M., Ghaemi, A., Arjomandi, H.: Experimental, Kinetics and Isothermal Modeling of Carbon Dioxide Adsorption with 13X Zeolite in a Fixed Bed Column. Iran. J. Chem. Eng. 16, 54–64 (2019).
31. Khodadadi, A., Torabi angajia, M., Talebizadeh rafsanjania, A., Yonesi, A.: Adsorptive desulfurization of diesel fuel with nano copper oxide (CuO). Proc. 4th Int. Conf. Nanostructures. 2, 12–14 (2012).
32. Khodadadi Dizaji, A., Mortaheb, H.R., Mokhtarani, B.: Complete oxidative desulfurization using graphene oxide-based phosphomolybdic acid catalyst: Process optimization by two phase mass balance approach. Chem. Eng. J. 335, 362–372 (2018).
33. Kumagai, S., Ishizawa, H., Toida, Y.: Influence of solvent type on dibenzothiophene adsorption onto activated carbon fiber and granular coconut-shell activated carbon. Fuel. 89, 365–371 (2010).
34. Lecrenay, E., Sakanishi, K., Mochida, I.: Catalytic hydrodesulfurization of gas oil and model sulfur compounds over commercial and laboratory-made CoMo and NiMo catalysts: Activity and reaction scheme. Catal. Today. 39, 13–20 (1997).
35. Leofanti, G., Padovan, M., Tozzola, G., Venturelli, B.: Surface area and pore texture of catalysts. Catal. Today. 41, 207–219 (1998).
36. Li, H., Liu, J., Li, J., Hu, Y.: Promotion of the Inactive Iron Sulfide to an Efficient Hydrodesulfurization Catalyst. ACS Catal. 7, 4805–4816 (2017).
37. Li, J., Lu, H., Tang, X., Zhou, M., Hu, N.: A novel method of preparation-adsorption desulfurization process for dibenzothiophene over sawdust-derived nickel/activated carbon. Pet. Sci. Technol. 36, 456–462 (2018).
38. Luo, J., Xiong, J., Chao, Y., Li, X., Li, H., Pang, J., Zhu, F., Zhu, W., Li, H.: Activated boron nitride ultrathin nanosheets for enhanced adsorption desulfurization performance. J. Taiwan Inst. Chem. Eng. 93, 245–252 (2018).
39. Mafi, M., Dehghani, M.R., Mokhtarani, B.: Liquid-liquid equilibrium data for extractive desulfurization using 1-butyl-3-methyl imidazolium thiocyanate, n- alkane and thiophene. Fluid Phase Equilib. 456, 109–115 (2018).
40. Mafi, M., Mokhtarani, B., Dehghani, M.R.: Removal of thiophene from model diesel oil with nitrate based ionic liquids at several temperatures. J. Mol. Liq. 221, 1104–1110 (2016).
41. Magistri, L., Bozzolo, M., Tarnowski, O., Agnew, G., Massardo, A.F.: Design and Off-Design Analysis of a MW Hybrid System Based on Rolls-Royce Integrated Planar SOFC. ASME Pap. No. GT2003-38220. 129, (2003).
42. Mandizadeh, S., Sadri, M., Salavati-Niasari, M.: Mechanosynthesis and characterization AFe_2O_4 (A: Ni, Cu, Zn)-activated carbon nanocomposite as an effective adsorbent for removal dodecanethiol. Microporous Mesoporous Mater. 262, 13–22 (2018).
43. Mei, H., Mei, B.., Yen, T.F.: A new method for obtaining ultra-low sulfur diesel fuel via ultrasound assisted oxidative desulfurization. Fuel. 82, 405–414 (2003).
44. Moosavi, E.S., Dastgheib, S.A., Karimzadeh, R.: Adsorption of Thiophenic Compounds from Model Diesel Fuel Using Copper and Nickel Impregnated Activated Carbons. Energies. 5, 4233–4250 (2012).
45. Moradi, M., Karimzadeh, R., Moosavi, E.S.: Modified and ion exchanged clinoptilolite for the adsorptive removal of sulfur compounds in a model fuel: New adsorbents for desulfurization. Fuel. 217, 467–477 (2018).
46. Moreno-castilla, C., Carrasco-marín, F., Maldonado-hódar, F.J., Rivera-utrilla, J.: Effects of non-oxidant and oxidant acid treatments on the surface properties of an activated carbon with very low ash content. Carbon N. Y. 36, 145–151 (1998).
47. Morozov, I.V., Znamenkov, K.O., Korenev, Y.M., Shlyakhtin, O.A.: Thermal decomposition of $Cu(NO_3)_2 \cdot 3H_2O$ at reduced pressures. Thermochim. Acta. 403, 173–179 (2003).
48. Nazal, M.K., Oweimreen, G.A., Khaled, M., Atieh, M.A., Aljundi, I.H., Abulkibash, A.M.: Adsorption isotherms and kinetics for dibenzothiophene on activated carbon and carbon nanotube doped with nickel oxide nanoparticles. Bull. Mater. Sci. 39, 437–450 (2016).
49. Oloruntoba, M., Aribike, D., Nwachukwu, S.: A Review on Bio- And Adsorptive Desulfurization of Diesel Fuel. J. Sci. Res. Reports. 11, 1–6 (2016).
50. Panahi, R.: determination of adsorption isotherm for L-Lysine imprinted polymer. Iran. J. Chem. Eng. 5, 49–55 (2008).

51. Safa, M., Mokhtarani, B., Mortaheb, H.R.: Deep extractive desulfurization of dibenzothiophene with imidazolium or pyridinium-based ionic liquids. Chem. Eng. Res. Des. 111, 323–331 (2016)(a).
52. Safa, M., Mokhtarani, B., Mortaheb, H.R., Tabar Heidar, K.: Oxidative Desulfurization of Model Diesel Using Ionic Liquid 1-Octyl-3-methylimidazolium Hydrogen Sulfate: An Investigation of the Ultrasonic Irradiation Effect on Performance. Energy & Fuels. 30, 10909–10916 (2016)(b).
53. Safa, M., Mokhtarani, B., Mortaheb, H.R., Tabar Heidar, K., Sharifi, A., Mirzaei, M.: Oxidative Desulfurization of Diesel Fuel Using a Brønsted Acidic Ionic Liquid Supported on Silica Gel. Energy & Fuels. 31, 10196–10205 (2017).
54. Samokhvalov, A., Tatarchuk, B.J.: Review of Experimental Characterization of Active Sites and Determination of Molecular Mechanisms of Adsorption, Desorption and Regeneration of the Deep and Ultradeep Desulfurization Sorbents for Liquid Fuels. Catal. Rev. 52, 381–410 (2010).
55. Sano, Y.: Adsorptive removal of sulfur and nitrogen species from a straight run gas oil over activated carbons for its deep hydrodesulfurization. Appl. Catal. B Environ. 49, 219–225 (2004).
56. Seifikar Gomi, L., Afsharpour, M.: Porous MoO_3@SiC hallow nanosphere composite as an efficient oxidative desulfurization catalyst. Appl. Organomet. Chem. 33, e4830 (2019).
57. Seredych, M., Bandosz, T.J.: Adsorption of Dibenzothiophenes on Nanoporous Carbons: Identification of Specific Adsorption Sites Governing Capacity and Selectivity. Energy & Fuels. 24, 3352–3360 (2010).
58. Shalaby, C., Ma, X., Zhou, A., Song, C.: Preparation of Organic Sulfur Adsorbent from Coal for Adsorption of Dibenzothiophene-type Compounds in Diesel Fuel. Energy & Fuels. 23, 2620–2627 (2009).
59. Song, H., Yang, G., Song, H.-L., Wang, D., Wang, X.-Q.: Preparation of Ag/TiO_2-zeolite adsorbents, their desulfurization performance, and benzothiophene adsorption isotherms. Russ. J. Phys. Chem. A. 91, 390–397 (2017).
60. Vilarrasa-García, E., Infantes-Molina, A., Moreno-Tost, R., Rodríguez-Castellón, E., Jiménez-López, A., Cavalcante, C.L., Azevedo, D.C.S.: Thiophene adsorption on microporous activated carbons impregnated with $PdCl_2$. Energy and Fuels. 24, 3436–3442 (2010).
61. Wang, Y., Yang, R.T.: Desulfurization of Liquid Fuels by Adsorption on Carbon-Based Sorbents and Ultrasound-Assisted Sorbent Regeneration. Langmuir. 23, 3825–3831 (2007).
62. Zhang, P., Mao, X., Yang, B.: Mechanistic Study on Adsorption Desulfurization Using Modified Graphene. Ind. Eng. Chem. Res. 3, 41 (2019).

Figures

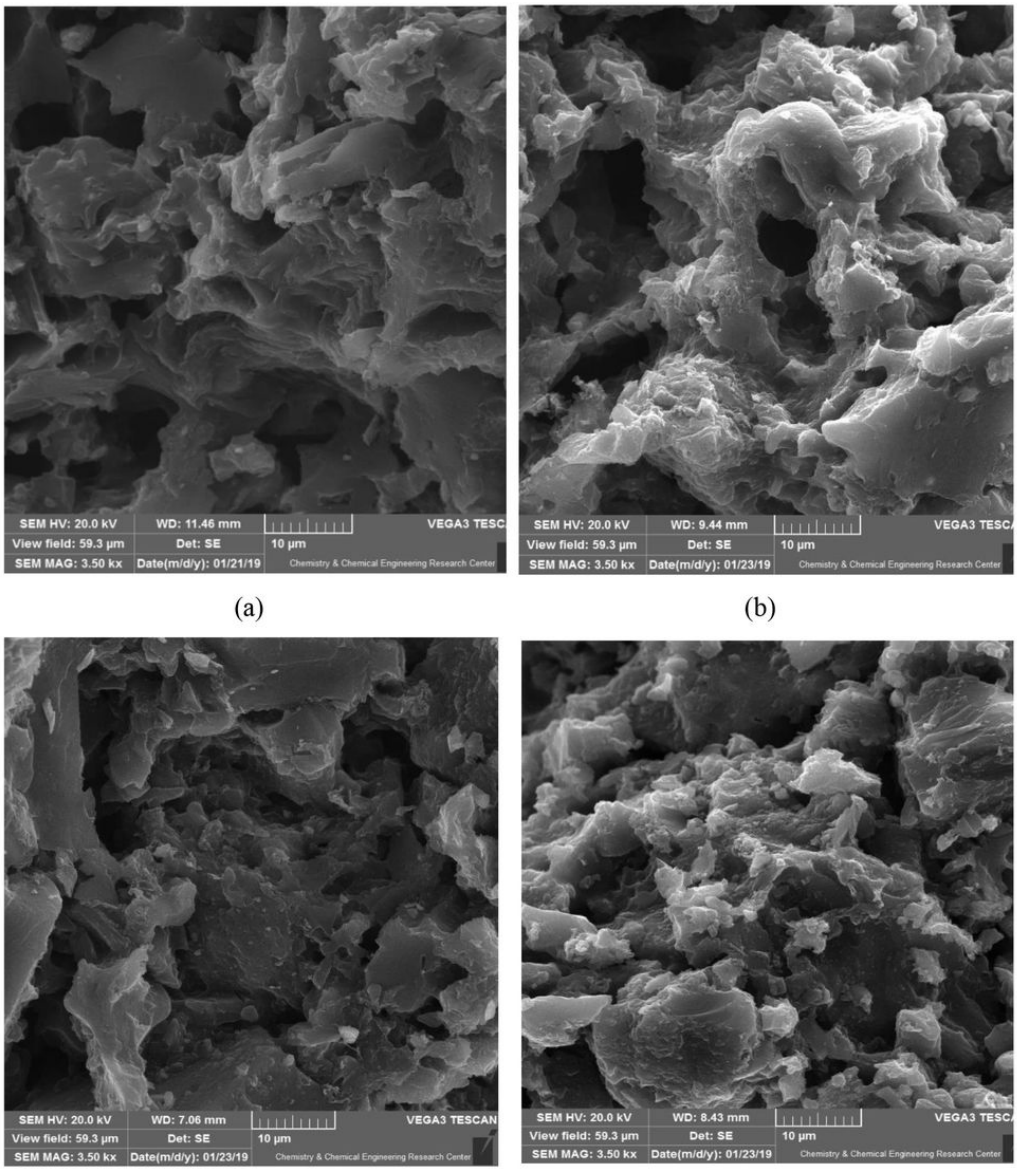

Figure 1

SEM images with a magnification of 3500× and a 10 µm particle size of, a) AC, b) ACN, c) A1CN10 (before adsorption operation), d) A1CN10 (after adsorption operation)

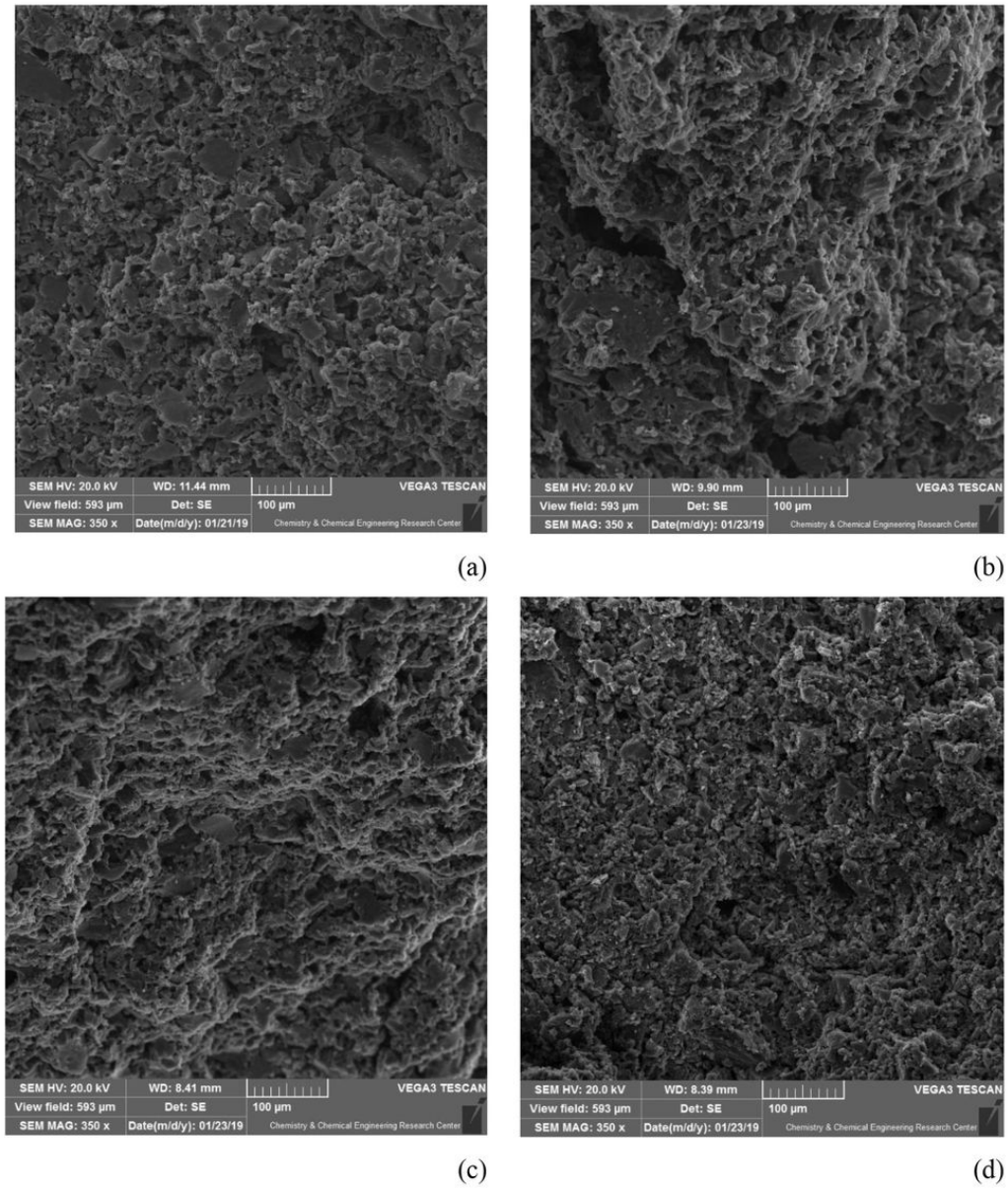

Figure 2

SEM images with a magnification of 350× and a 100 µm particle size of, a) AC, b) ACN, c) A1CN10 (before adsorption operation), d) A1CN10 (after adsorption operation)

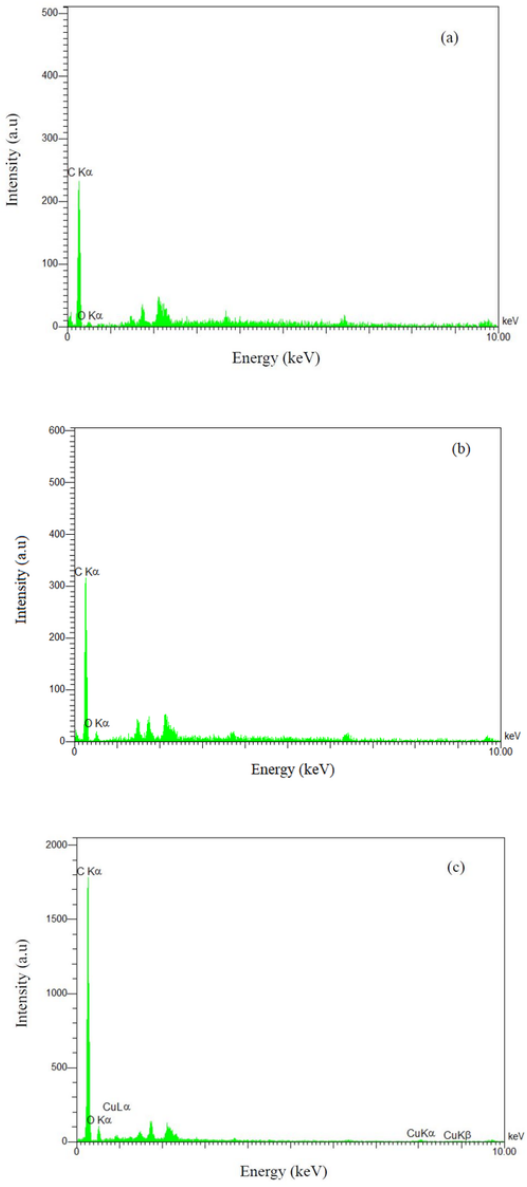

Figure 3

Results of EDS analysis for adsorbents, a) AC, b) ACN c) A1CN10

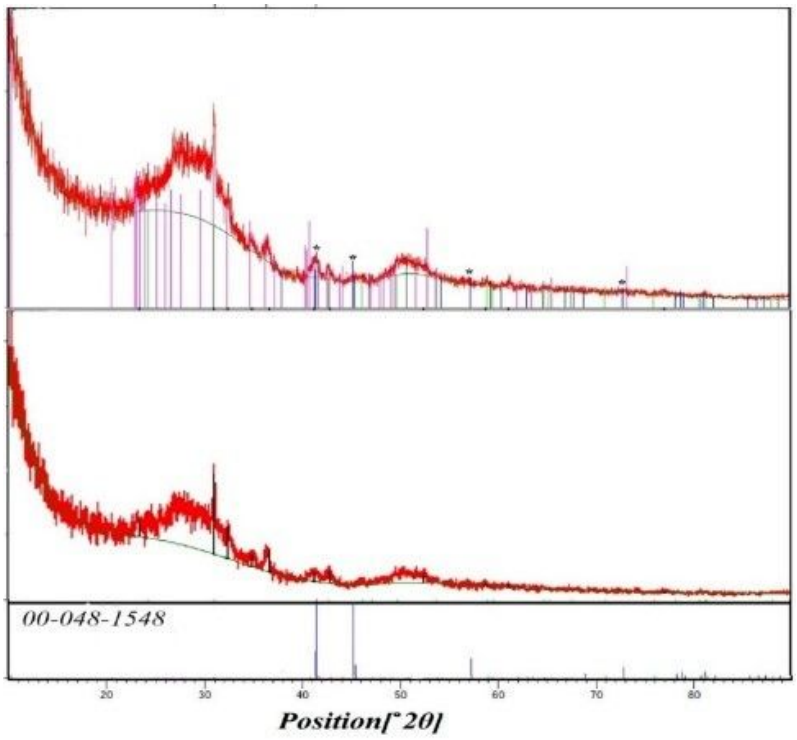

Figure 4

Results of XRD analysis of AC before (bottom) and after loading Cu(II) (top)

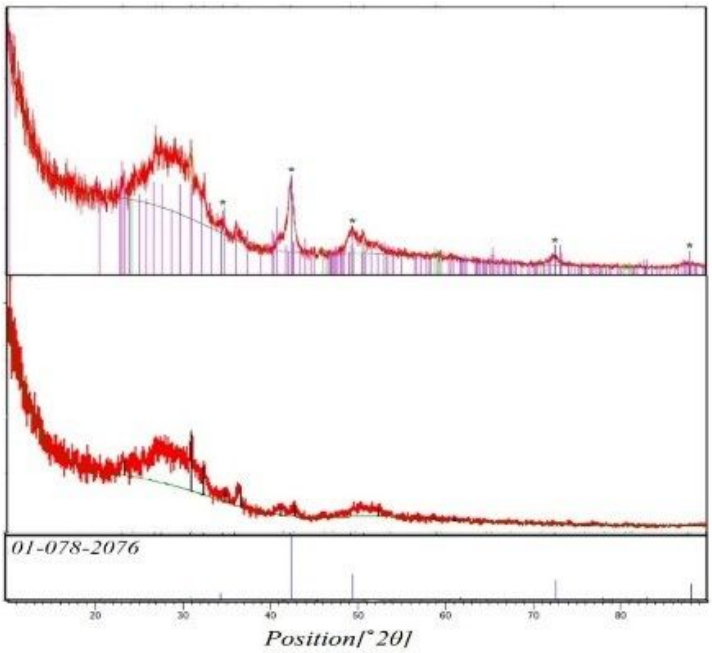

Figure 5

Results of XRD analysis of AC before (bottom) and after loading Cu(I) (top)

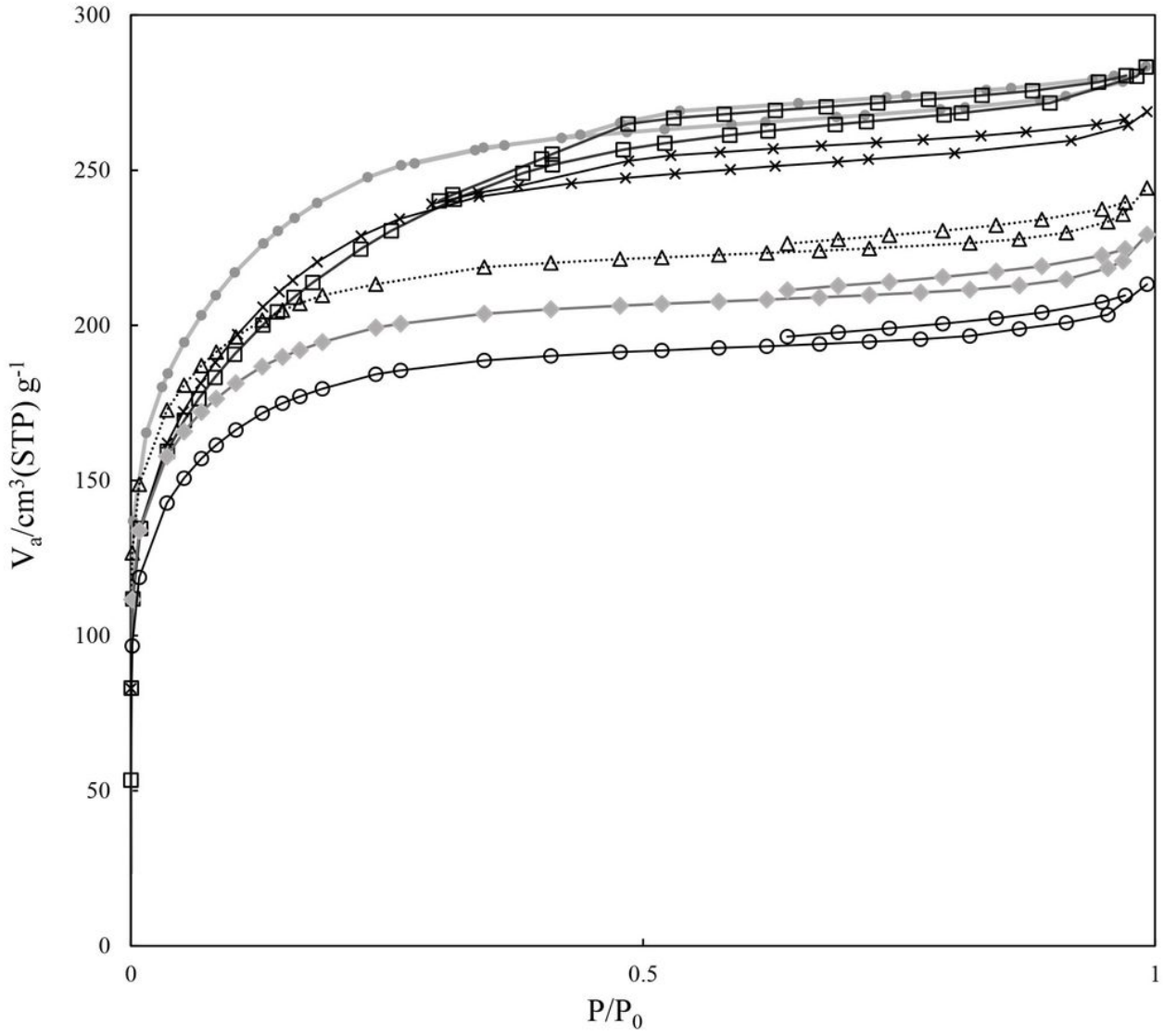

Figure 6

N_2 adsorption-desorption isotherms of ●) AC,) ACS, □) ACN, Δ) A1C, ♦) A1CN10, ●) A2CN10

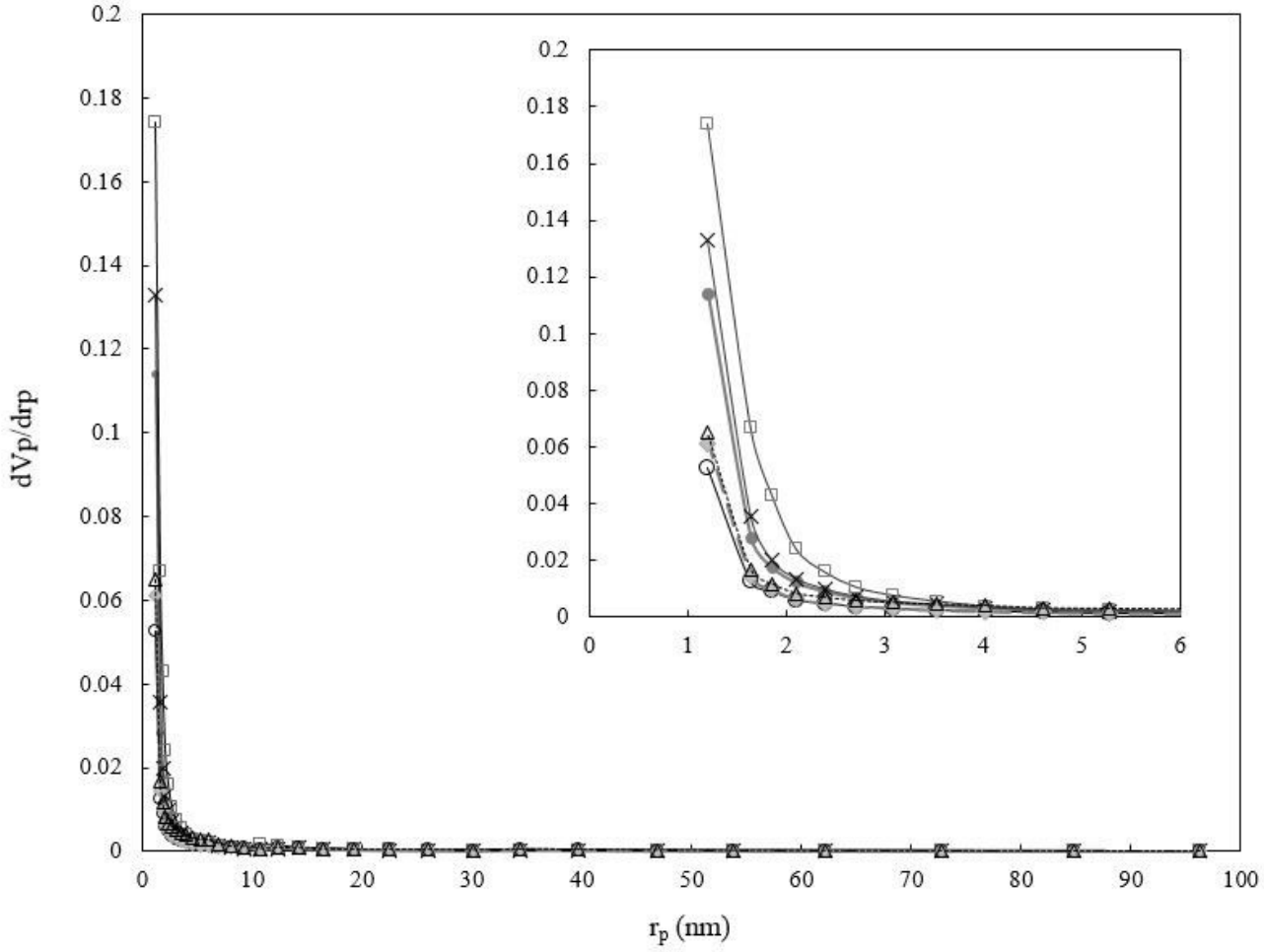

Figure 7

Pore size distribution of □) ACN,) ACS, ●) AC, Δ) A1C, ♦) A1CN10, ●) A2CN10

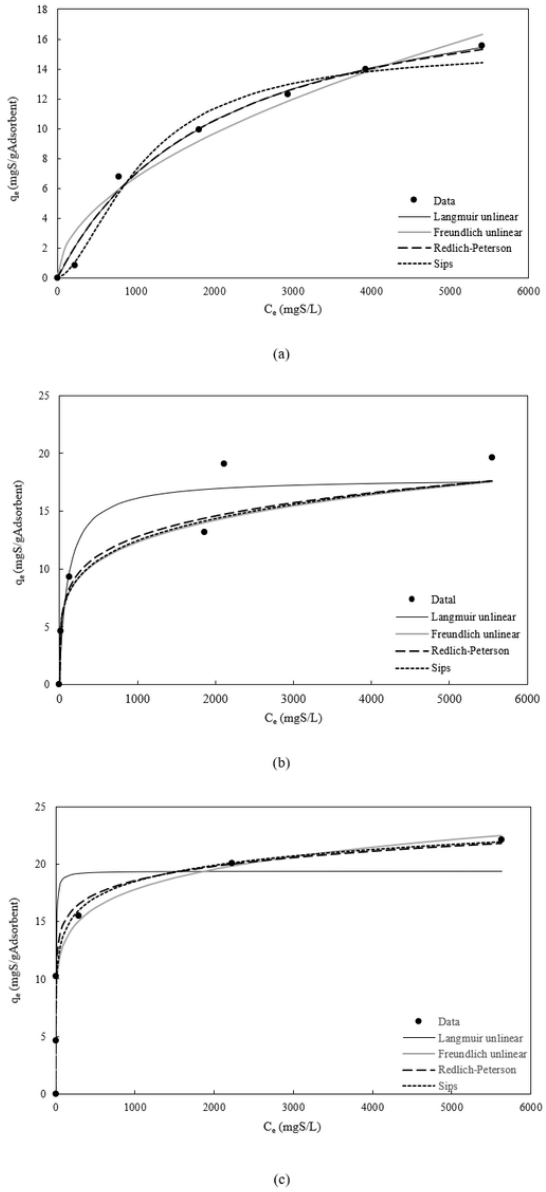

Figure 8

Adsorption isotherms of (A) T-Hex, (B) BT-Hex, (C) DBT-Hex, on A1CN10

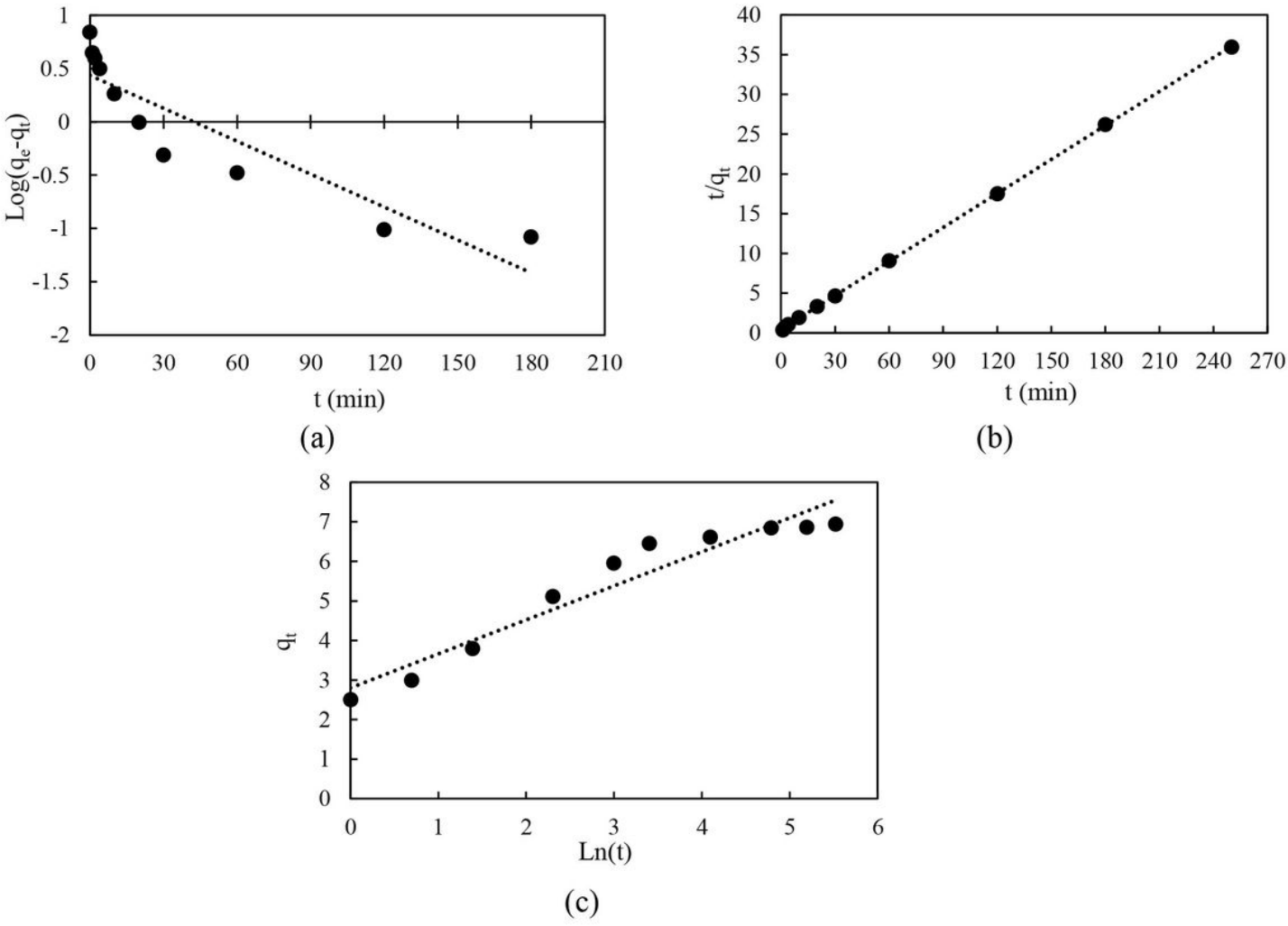

Figure 9

Diagrams of fitted Models of adsorption kinetic data for the hexane-thiophene solution by A1CN10, a) pseudo-first-order, b) pseudo-second-order, c) Elovich

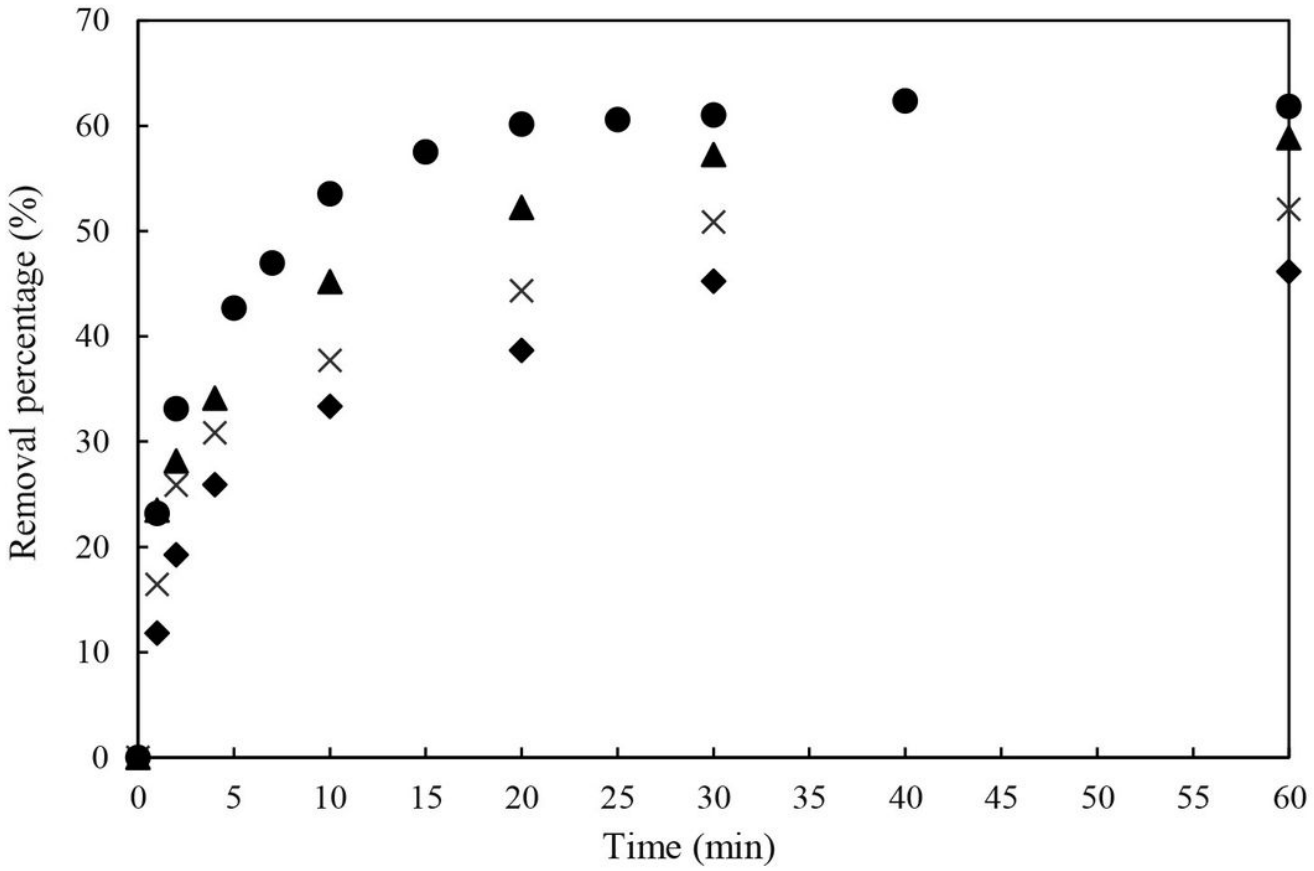

Figure 10

Effect of Cu loading treatments on thiophene removal from n-hexane, ♦) AC,) AC350, ▲) A2C, ●) A1C

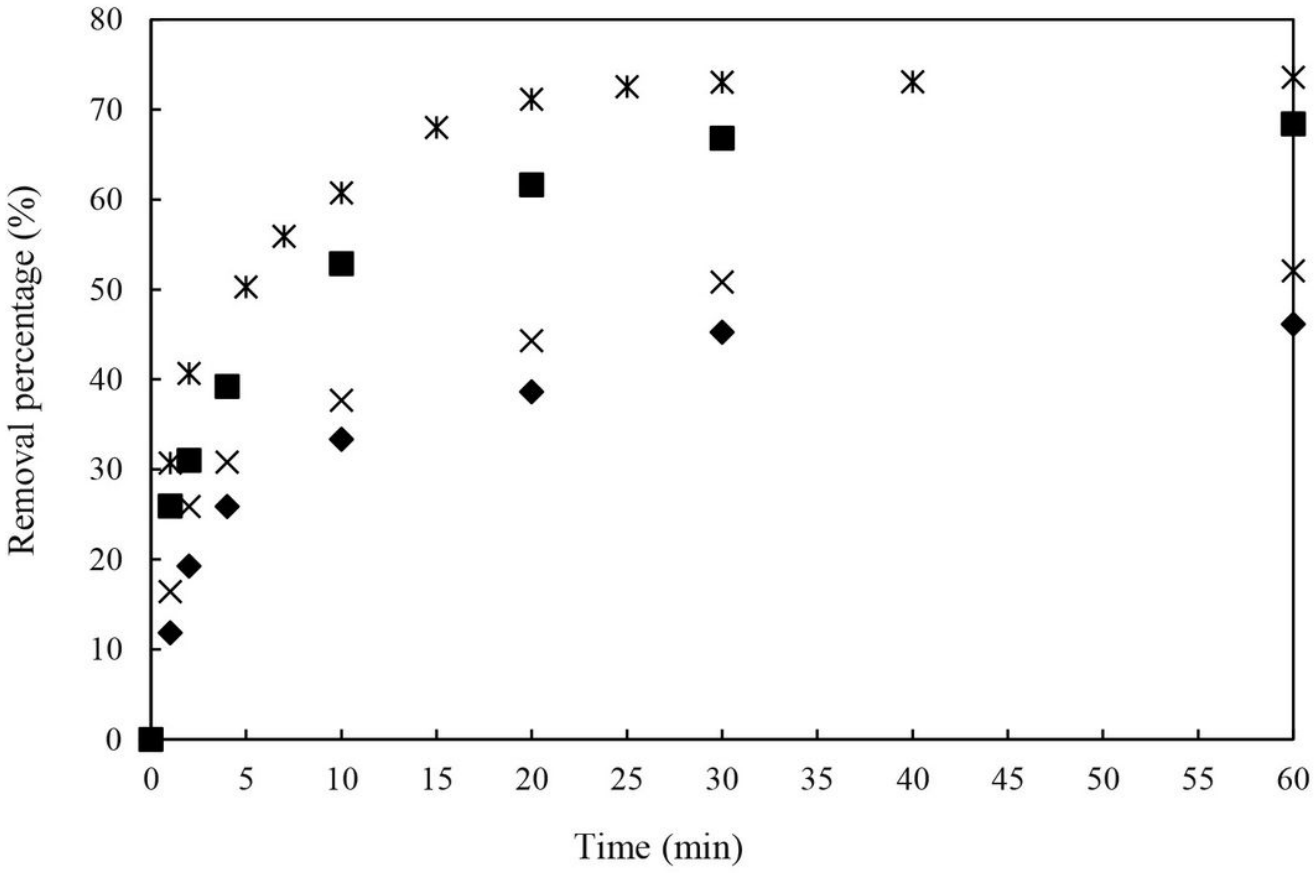

Figure 11

Effect of acid washing treatments on the removal of thiophene in n-hexane, ♦) AC,) AC350, ■) ACS, Ж) CAN

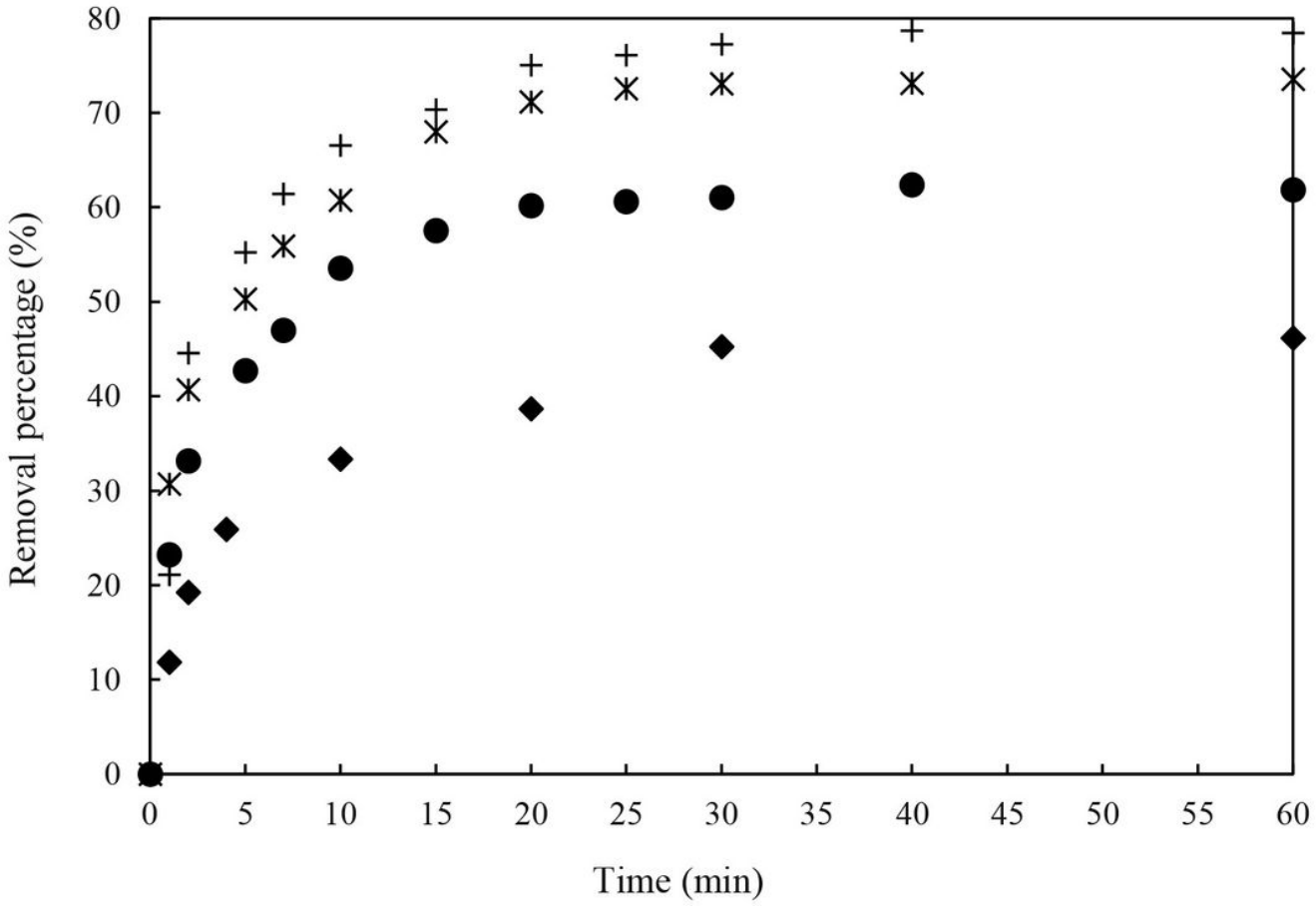

Figure 12

Effect of treatments on the removal of thiophene in n-hexane by: ♦) AC, ●) A1C, Ж) ACN, +) A1CN10

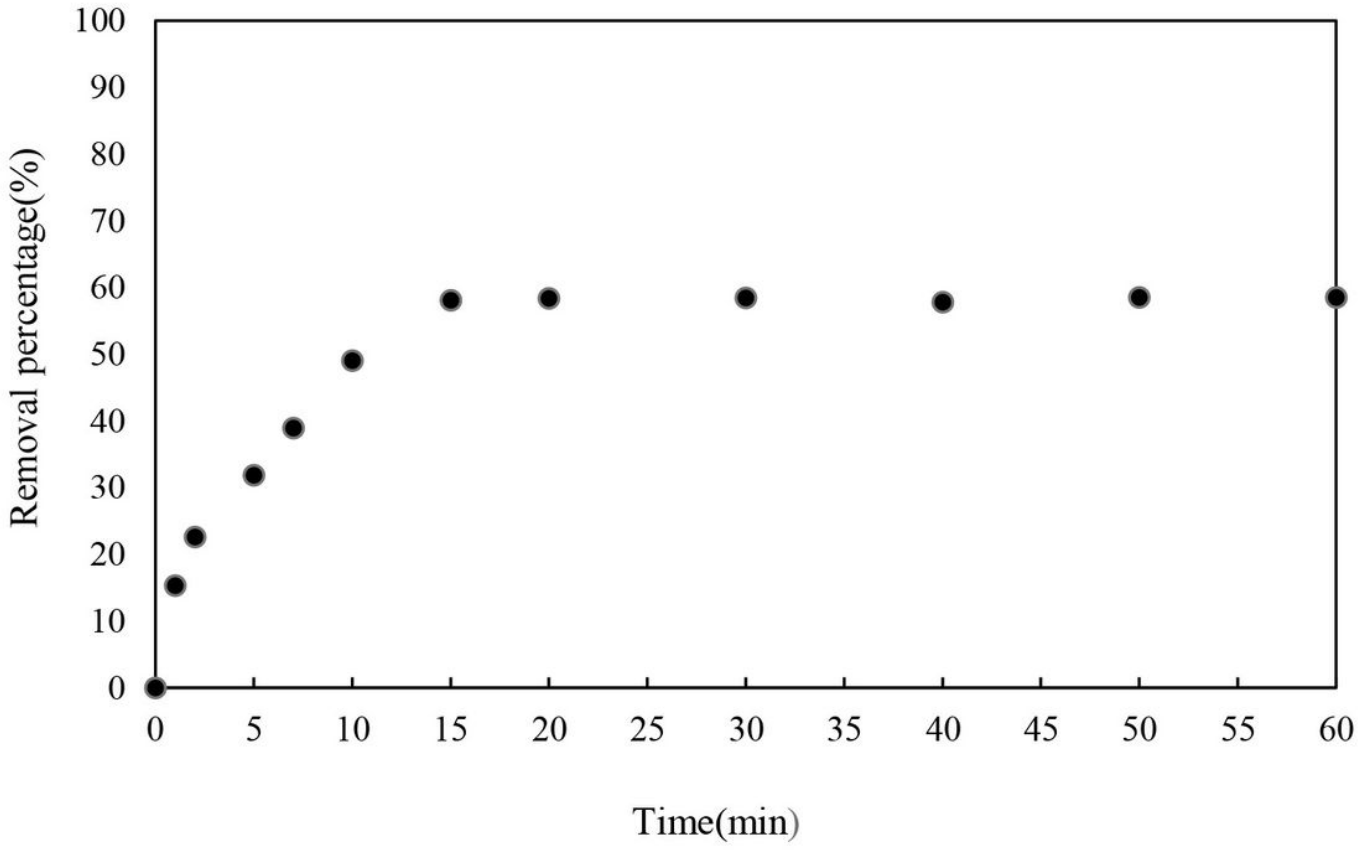

Figure 13

Thiophene removal from kerosene by A1CN10 with 2000 ppm initial concentration

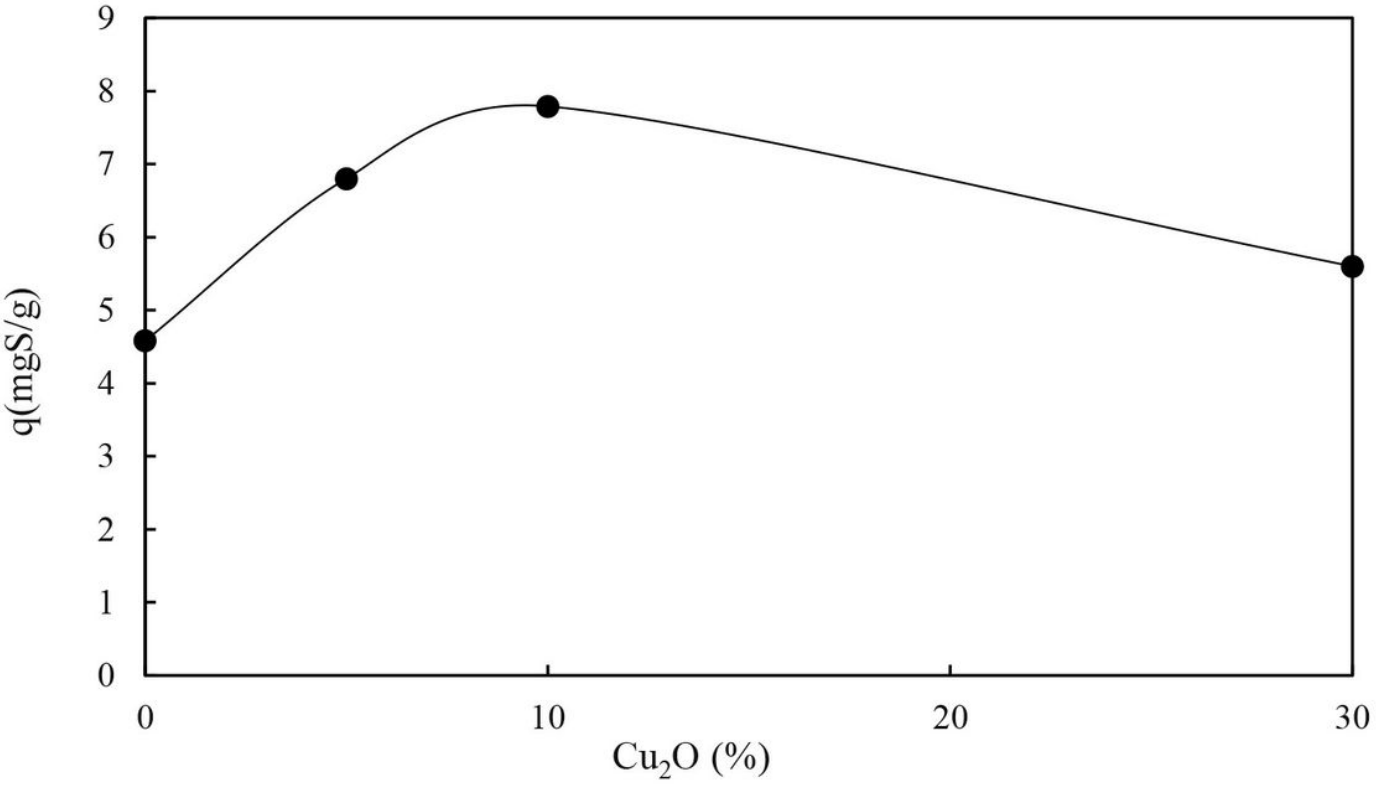

Figure 14

The effect of different amounts of Cu(I) loading on AC adsorption capacity for removing thiophene from n-hexane solution

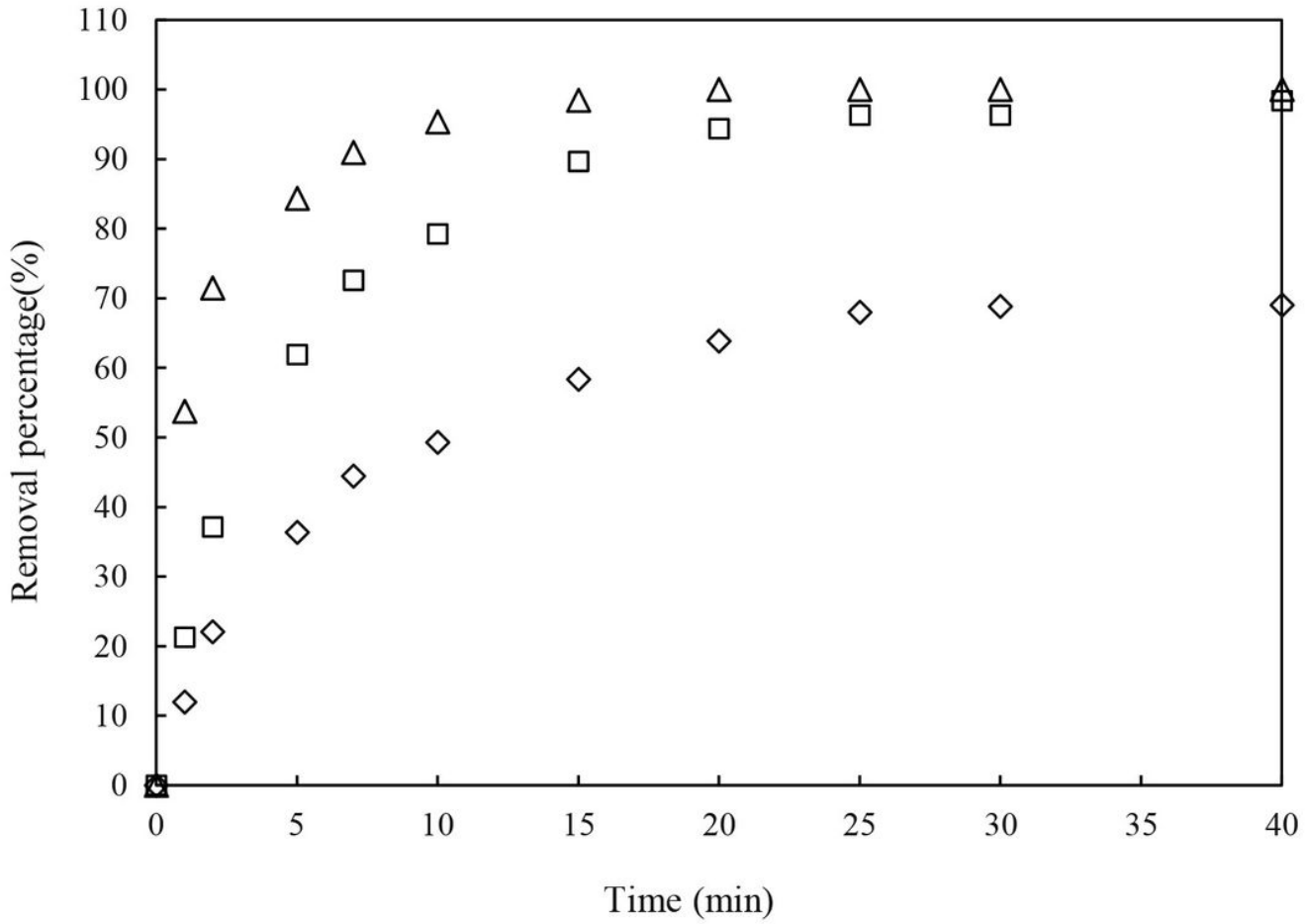

Figure 15

Removal percentage of mixture components (T, BT, and DBT) in n-hexane on A1CN10. (initial concentration: 1000ppmT, 1000ppmBT, 1000ppmDBT), Δ) DBT, □) BT, ◊) T